NASA CONTRACTOR
    REPORT
    RE-468


AVOIDANCE OF STRESS CORROSION SUSCEPTIBILITY

IN HIGH STRENGTH ALUMINUM ALLOYS BY CONTROL

OF GRAIN BOUNDARY AND MATRIX MICROSTRUCTURE


Prepared for Contract No. NAS 8-28986 by

Philip Adler

and

Richard DeIasi

Research Department
Grumman Aerospace Corporation
Bethpage, New York   11714

for


NASA-GEORGE C. MARSHALL SPACE FLIGHT CENTER
HUNTSVILLE, ALABAMA

January 1974

AVOIDANCE OF STRESS CORROSION SUSCEPTIBILITY

IN HIGH STRENGTH ALUMINUM ALLOYS BY CONTROL

OF GRAIN BOUNDARY AND MATRIX MICROSTRUCTURE


by

Philip Adler

and

Richard DeIasi

Prepared for Contract No. NAS 8-28986 by

GRUMMAN AEROSPACE CORPORATION
Research Department
Bethpage, New York   11714

for

NATIONAL AERONAUTICS AND SPACE ADMINISTRATION
George C. Marshall Space Flight Center
Astronautics Laboratory
Materials Division
Huntsville, Alabama


Approved by: *Charles E. Mack Jr.*
Charles E. Mack, Jr.
Director of Research

# FOREWORD

## ABSTRACT

This report describes an investigation of the role of microstructure to the mechanical strength and stress corrosion resistance of highest strength and overaged tempers of recently developed BAR and 7050 aluminum alloys. Comparison is made with previously studied 7075 aluminum alloy. Optical microscopy, transmission electron microscopy, and differential scanning calorimetry were used to characterize the grain morphology, matrix microstructure, and grain boundary microstructure of these tempers. The highest strength temper of 7050 was found to exhibit unusually high strength in relation to its matrix microstructure, and strengthening, based on a relatively uniform matrix precipitate size, is suggested. Results of stress corrosion testing to evaluate crack initiation, crack propagation, and overall time-to-failure in an aqueous chloride environment over a 0.7 to 3.4 pH range are reported, and a comparison is made with alternate immersion test results obtained in 6.8 to 8.2 pH environments. Grain boundary interparticle spacing was significant to stress corrosion crack propagation for all three alloys; increasing interparticle spacing led to increased resistance to crack propagation. In addition, the finer grain size in BAR and 7050 in comparison to 7075 appears to enhance crack propagation. The highest strength temper of 7050 has a comparatively high resistance to crack initiation. Overall stress corrosion behavior is dependent on environment pH, and evaluation over a range of pH is recommended.

# TABLE OF CONTENTS

Preceding page blank

# LIST OF ILLUSTRATIONS

# LIST OF TABLES

# 1. INTRODUCTION

The most serious limitation on the use of high-strength aluminum alloys is their susceptibility to stress corrosion (Refs. 1 and 2). For 7000 series commercial alloys these problems can be virtually avoided through the use of lower strength tempers (Refs. 3 and 4); still, this trade off precludes the attainment of the maximum capabilities of these alloys. And such a goal will not be reached until the factors responsible for stress corrosion are understood. The investigation described in this report was aimed at clarifying the significance of microstructure to both the stress corrosion susceptibility and mechanical strength of two recently developed high-strength aluminum alloys, BAR and 7050. Our earlier work on 7075 aluminum alloy (Ref. 5) indicated that grain boundary microstructure precipitate spacing is of primary importance in the propagation of stress corrosion cracks. Since the mechanical strength of this alloy was found to be primarily dependent upon matrix microstructure (Refs. 5-8), it appeared possible to produce highest strength material that is not susceptible to stress corrosion attack when both matrix and grain boundary microstructures are simultaneously controlled.

In this work, our focus is on recently developed 7050 and BAR aluminum alloys because study of these 7000 series alloys enables a more comprehensive understanding of the role of microstructure in stress and mechanical strength behavior than that obtained previously for 7075 aluminum alloy (Refs. 5, 6, and 9) and should provide a basis for evaluating these newer alloys. This effort comprises a literature survey concerning the significance of microstructure to mechanical properties and stress corrosion susceptibility, preparation of 7050 and BAR alloys in their highest strength and overaged tempers, evaluation of the mechanical properties of these four tempers, evaluation of their matrix and grain boundary microstructure using transmission electron microscopy, grain size analysis using optical microscopy, and evaluation of their matrix microstructure using thermal analysis. Comparison is made with previously obtained results for the highest strength and overaged tempers of 7075. Stress corrosion testing (pH 0.7-3.4)

1

on the highest strength and overaged tempers of BAR and 7050
was performed, and the results were compared with our previ-
ous results for 7075.  In addition, alternate immersion
stress corrosion testing was conducted by the COR on the
highest strength and overaged tempers of all three alloys
(pH 6.8-8.2).  These data provide a basis of comparison
with the results obtained at lower  pH.

# 2. LITERATURE SURVEY

## A. Significance of Microstructure to Mechanical Properties

The commercial 7000 series, Al-Mg-Zn type alloys, derive their highest strengths as a result of precipitation reactions accompanying heat treatment. Precipitation is generally recognized to take place in the following sequence (Refs. 1, 10, 11, and 12):

$$\text{Supersaturated Solid Solution} \rightarrow$$
$$\text{Guinier-Preston (G.P.) Zones} \rightarrow \eta'(MgZn_2) \rightarrow \eta(MgZn_2) \ .$$

The semicoherent intermediate $MgZn_2$ phase, $\eta'$, has been described as having a monoclinic unit cell (Ref. 13) while the incoherent equilibrium $MgZn_2$ phase, $\eta$, is hexagonal (Refs. 1 and 12).

Highest strength in 7000 series alloys has been found to coincide with a matrix containing G.P. zones and slight amounts of $\eta'$ phase (Refs. 5-7). Although G.P. zones have been suggested as the source of optimum strengthening (Refs. 8 and 14), maximum strength has also been attributed to other matrix structures, such as a matrix containing preponderant amounts of $\eta'$ (Ref. 10), the disappearance of G.P. zones (Ref. 15), and the appearance of equilibrium $\eta$ (Ref. 16).

Mechanical property enhancement in 7075 has been observed by reduction of the concentration of undesirable second phase particles that normally are present in this alloy (Refs. 17 and 18). Increased yield and ultimate strength, as well as ductility, were reported (Ref. 17). Reduction of the volume of second phase particles from 0.9 to 0.1 percent improved the ductility of short transverse specimens, $K_{Ic}$ fracture toughness, and fatigue characteristics in the short transverse direction (Ref. 18).

Ductility generally decreases with increased yield strength for 7000 series alloys. However, appropriate thermomechanical treatment can increase strength without a

reduction in ductility (Ref. 19). This is attributed to a combined strengthening effect related to dislocations and precipitation. Ductility has been found to increase with increasing width of the precipitate-free-zone (PFZ) at grain boundaries in an Al-Mg-Zn alloy (Ref. 20). However, no effect of PFZ width on total elongation was observed for highest strength 7075(5). Ductility has also been found to be a function of grain boundary precipitates for an Al-Mg-Zn alloy at constant strength (Ref. 21).

Fracture toughness in 7075, as indicated by crack propagation energy, was found to be related to grain boundary precipitate structure for an intergranular fracture mode (Ref. 22). On the other hand, yield strength, tensile strength, fatigue strength, fatigue crack propagation, and fracture toughness have been found to correlate with the size of matrix precipitates (Ref. 23). The role of different aspects of microstructure to many of the mechanical properties of 7000 series alloys, therefore, still appears uncertain. However, some relationships do appear valid, such as that between matrix microstructure and strength and that between elimination of undesirable second phase particles and property enhancement.

## B. Significance of Microstructure to Stress Corrosion

Study of the significance of different material parameters to stress corrosion attack in Al-Mg-Zn type alloys has focused on three principal microstructural features: 1) the precipitate-free-zone (PFZ), which forms adjacent to high angle grain boundaries, 2) matrix precipitate structure, and 3) grain boundary precipitate structure. The relative importance of these features is still controversial.

Results of early work indicated that the PFZ enhanced stress corrosion susceptibility (Refs. 10 and 24-26); however, more recent studies show that wide zones are preferred since they are weaker than the matrix and undergo preferential plastic deformation (Refs. 27 and 28). It has also been suggested that the solute content of the PFZ (indirectly related to the PFZ width) is important to stress corrosion susceptibility (Ref. 21), and that segregation of Zn and Mg in the grain boundary region increases corrosion potential (Ref. 29). Others contend the PFZ is not significant to stress corrosion attack (Refs. 5 and 30-32).

4

Matrix precipitate structure has also been suggested as the source of susceptibility (Refs. 30, 31, and 33-35). This line of argument is based on the mode of precipitate-dislocation interaction during plastic deformation which, in turn, is dependent upon precipitate coherency. This argument leads to the conclusion that the susceptibility of highest strength 7075 is a result of the presence of coherent G.P. zones and semicoherent intermediate $\eta'$, while the nonsusceptibility of overaged material is due to the presence of $\eta'$ and incoherent $\eta$. The general dependence of stress corrosion susceptibility on aging conditions is explainable in this manner. This argument would eliminate the possibility of attaining highest strength material that is not susceptible.

Our work (Refs. 5 and 36) and that of Kent (Refs. 37 and 38) support the Unwin and Nicholson contention (Ref. 39) that the precipitate structure at the grain boundary is of principal importance to stress corrosion susceptibility. A maximum coverage of grain boundary area by precipitates and a minimum spacing of grain boundary particles was felt to coincide with maximum susceptibility (Ref. 39).

## C.   Recently Developed BAR and 7050 Alloys

The overall objectives in the development of BAR and 7050 alloys were to enhance the properties by  1) increasing the strength of thicker sections,  2) improving the resistance to stress corrosion attack, and  3) increasing the fracture toughness (Refs. 40-47).  (A recent designation of RX720 has been given the BAR alloy; the 7050 alloy was originally termed MA15.)  The development of these alloys was based on studies of the role of minor addition elements on quench sensitivity (Refs. 48-55).  It was found that  Cr was a major factor contributing to quench sensitivity, and by substitution of  Zr  for  Cr,  quench sensitivity could be reduced substantially while maintaining the desired recrystallization suppressing effect of  Cr.  By reducing quench sensitivity, thicker sections of higher strength could be fabricated.  In addition, other improvements in mechanical properties and stress corrosion resistance were observed.

The BAR material was developed by the Reynolds Metals Company in cooperation with the Boeing Company under Air Force sponsorship (Refs. 40-42); the 7050 alloy was developed by Alcoa under Naval Air Systems Command and Air Force sponsorship (Refs. 43-47). Alloy chemistry appears to be the major difference between these alloys (see Table 1). Both alloys have approximately the same Zr

TABLE 1  ELEMENTAL ANALYSIS OF ALUMINUM ALLOYS

| Alloy | Composition (wt %) | | | | | | | | | |
|-------|------|-----|-----|-------|------|------|------|-------|------|-----|
|       | Zn | Mg | Cu | Zr | Cr | Si | Fe | Ti | Mn | Al |
| BAR   | 7.2 | 2.4 | 1.4 | 0.094 | N.D. | 0.07 | 0.08 | 0.025 | N.D. | REM |
| 7050  | 6.2 | 2.2 | 2.3 | 0.086 | N.D. | 0.07 | 0.06 | 0.029 | 0.03 | REM |
| 7075  | 6.1 | 2.4 | 1.6 | N.D.  | 0.20 | 0.11 | 0.20 | 0.036 | 0.04 | REM |

content, substituted for Cr, but BAR alloy has a higher Zn and lower Cu content than the 7050 alloy. These differences in Zn and Cu content should result in differing mechanical and stress corrosion properties since higher Zn content improves resistance to stress corrosion, but increases quench sensitivity (Ref. 53), whereas increased Cu content enhances mechanical strength and resistance to stress corrosion (Refs. 1, 49, 53, and 55). The 7050 alloy is commercially available and has higher strength, better fracture toughness, i.e., higher $K_{Ic}$, and superior stress corrosion resistance than 7075 (Ref. 56). BAR has been found to have a good combination of strength and $K_{Ic}$, but its resistance to stress corrosion attack in alternate immersion testing, while better than 7075-T6, is not impressive (Ref. 40).

# 3. EXPERIMENTAL

## A. Sample Description

Samples of 7050 were taken from a 15.2 cm (6-in.) thick hand forging supplied by Alcoa; BAR samples were obtained from a 7.6 cm (3-in.) thick rolled plate stock supplied by the Reynolds Metals Company. The composition of the materials, as determined by the Grumman Quality Control Laboratory using X-ray fluorescence and emission spectroscopy, is listed in Table 1. Analysis of previously studied 7075 obtained in the form of 7.6 cm (3-in.) bar stock is included for comparison.

## B. Heat Treatment

The BAR material was received in its highest strength, T6 temper. Samples were overaged at 163°C as recommended by the supplier. Based on data shown in Table 2, a heat treatment of 21 hours at 163°C was selected for overaging this alloy to the T7 temper (Ref. 40).

### TABLE 2 EFFECT OF AGING TIME AT 163°C ON HARDNESS OF BAR ALLOY

| Time (hr) | Hardness (DPH - 5 kg) |
|---|---|
| "as-received" | 193 |
| 4 | 188 |
| 8 | 176 |
| 18 | 163 |
| 21 | 160 |
| 31 | 153 |

The 7050 alloy was received in the overaged T7352 temper. Recommended heat treatment to the highest strength temper is by solution heat treatment at 480°C for 2 hours,

7

aging at 120°C for 4 hours, followed by a 168°C aging for 4 hours (Ref. 56). Specimens were given this treatment and were water quenched following the solution heat treatment.

For previous work on 7075, samples were taken from a 7.6 cm (3-in.) thick rolled bar that was in the highest strength, stress relieved T651 temper. Individual specimens were overaged by heat treating at 175°C for 9 hours.

## C. Specimen Preparation

Samples were machined from 0.38 cm (0.150-in.) thick slices. "Dogbone" type, flat tensile specimens, 7.6 x 2.5 cm (3 x 1 in.), with a reduced center section 3.8 cm (1.50-in.) long by 1.270 cm (0.500 in.) wide by 0.127 cm (0.050 in.) thick were obtained from each slice. The uniaxial loading direction of the specimen, along the 7.6 cm (3-in.) dimension, was parallel to the short transverse direction of the bar or forging. These specimens were used for both mechanical property and stress corrosion susceptibility measurements.

Alternate immersion stress corrosion specimens [0.32 cm (1/8-in.) round bars] for each of the tempers of interest (highest strength and overaged — 7075, BAR, and 7050) were prepared in accordance with the Department of the Army Ordnance Corps Specification No. DS218. In all cases, the specimen loading direction was maintained in the short transverse direction.

## D. Mechanical Testing

The stress-strain behavior of each temper was measured and used to determine the 0.2 percent offset yield strength, tensile strength, and elongation. A minimum of four specimens from each temper tested at a crosshead speed of 5.1 cm/min (2.0 x $10^{-2}$ ipm).

Hardness was routinely used to evaluate the sample temper. Five Vickers diamond pyramid hardness (DPH, at a 5 kg load) impressions were made on each specimen. Impressions were made on surfaces that were final-polished using 1 $\mu$m alumina.

## E.  Electron Microscopy

Transmission microscopy was used to determine the microstructure of each sample condition.  Disks were punched from stress corrosion test specimens at areas adjacent to the exposed portion and thinned by twin jet-polishing, using a two-parts methanol, one-part nitric acid electrolyte at temperatures less than  -30°C  and at an applied voltage of 15V.  Examination was performed with a Phillips EM300 electron microscope.

## F.  Differential Scanning Calorimetry

To characterize the existing precipitate structure, calorimetric measurements were made using a duPont 900 Thermoanalyzer containing a differential scanning calorimeter (DSC) plug-in module.  This technique has been described (Ref. 57) and was previously applied to analysis of 7075 aluminum alloy (Ref. 6).  Sample disks of  0.56 cm  (7/32 in.) diameter x 0.127 cm  (0.050 in.) thickness were prepared from each of the six tempers under investigation.  To increase the sensitivity of the measurements, the heat flow was measured with respect to a high purity aluminum disk reference.  Runs were made at a heating rate of  10°C/min over the range from room temperature to  480°C.  Dried nitrogen  $(1 \times 10^{-4} \text{ m}^3/\text{min})$  was passed through the calorimeter to minimize oxidation.

## G.  Optical Microscopy

To characterize the grain size and anisotropy of BAR and 7050 alloys, photomicrographs of three specimens of each alloy were used for analysis.  Five photomicrographs at 690x magnification were taken of each specimen to ensure good statistics.  The grain size and anisotropy were found to be consistent within a particular alloy.

## H.  Stress Corrosion Testing

Smooth surface specimens were used so that both the initiation and propagation of cracking could be monitored.  Surface preparation consisted of metallographic polishing, using successive size grits to  1μm  alumina powder, electro-

polishing in three parts methanol/one part nitric acid at -40°C to -50°C, and final etching for 10 seconds with modified Keller's etch.

A specially constructed apparatus, described in Ref. 9, was used for stress corrosion testing. Essentially, the sample is held at a relatively constant load [3336N (750 lb) or an initial stress of 207 x $10^6$N/m$^2$ (30 ksi) for the studies herein described] while exposed to a continuously circulated test solution. During testing, microextension accompanying cracking and load on the specimen were continually monitored.

A three percent NaCl solution environment, buffered by 0.5 percent AlCl$_3$, was used throughout. A Teflon cell attached to the reduced center portion of the specimen served as a container for the test solution that continuously flowed over one specimen face, then the other, and returned to the reservoir. The window area over both specimen faces was 1.067 x 1.422 cm (0.420 x 0.560 in.). Fresh solution from a 1 x $10^{-3}$ m$^3$ (1-liter) reservoir was used for each test and was circulated by a nitrogen gas lift pump that also acted to purge dissolved oxygen from the solution. Hydrochloric acid was added to obtain desired initial acidity. A range from 0.7 to 3.4 pH was studied, the latter solution containing no acid addition. Solution pH was periodically checked during and after each test.

Microextension accompanying attack was used to monitor sample behavior. A linear variable differential transformer (LVDT) with a ±5.1 x $10^{-6}$ cm (±2 x $10^{-6}$ in.) sensitivity was attached to the specimen by knife edges. Extension in the direction of loading, which is normal to the direction of crack propagation, was continually recorded. In a typical test sequence, an initial period of no extension is followed by time-dependent changes. The time at which extension initiates is indicative of the time period prior to cracking and is termed the incubation period, $t_{inc}$. Time-dependent changes (cracking) occur, as indicated by the extension, until failure. The total time required to cause failure (TTF) is a measure of overall susceptibility.

10

Alternate immersion stress corrosion testing of the highest strength and overaged tempers of 7075, BAR, and 7050 aluminum alloys was conducted on 0.32 cm (1/8 in.) round bar specimens at the NASA Marshall Space Flight Center. Testing was performed at $172 \times 10^6$ and $310 \times 10^6$ N/m$^2$ (25 and 45 ksi) in either a 3.5 percent NaCl solution (pH 6.8-7.2) or synthetic seawater (pH 8.2) environment. The alternate immersion cycle consisted of 10 minutes in solution and 50 minutes in air.

# 4. RESULTS

## A. Mechanical Properties

A summary of the mechanical property test results is shown in Fig. 1. Previously determined results for 7075 are included for comparison.

The tensile specimens were loaded in the short transverse direction, and the results reflect the lower values normally associated with properties in this direction. A direct comparison between the materials shown in Fig. 1 would not be valid because of their differing wrought forms and "as-received" sizes. The 7075, BAR, and 7050 were obtained in the form of 7.6 cm (3-in.) rolled bar stock, 7.6 cm (3-in.) rolled sheet stock, and 15.2 cm (6-in.) hand forging, respectively. The 7050 would be expected to have higher mechanical properties [of the order of $20.7 \times 10^6$ N/m$^2$ (3 ksi) for yield and tensile strength (Ref. 44)] for 7.6 cm 3-in. thick material. Bearing these differences in mind, it appears that the 7050 alloy has significantly higher strength than BAR and 7075 in both the highest strength and overaged conditions, and overaged 7050-T7352 is almost comparable to highest strength 7075-T651. The properties of BAR and 7075 are generally comparable.

## B. Transmission Electron Microscopy

The microstructures of the overaged and highest strength tempers of 7075, BAR, and 7050 aluminum alloys are listed in Table 3. They represent an average of 10-15 electron micrographs taken from 3-5 separate specimens of each material. The data listed for 7075-T651 and -T7351 have been reported (Refs. 5 and 36) and are indicated for comparison with the more recently developed alloys. Representative electron micrographs of both tempers of 7075, BAR, and 7050 are shown in Figs. 2, 3, and 4, respectively. Several interesting matrix characteristics are immediately evident. The highest strength temper of both 7075 and BAR consists almost exclusively of G.P. zones with a small amount ($\sim$ 5%) of the semicoherent $\eta'$ phase. On the other hand, the highest strength temper of 7050 has a matrix consisting of approximately 50 percent G.P. zones, 50 percent $\eta'$, and

# TABLE 3   MICROSTRUCTURAL PROPERTIES OF ALUMINUM ALLOYS

| Property | Highest Strength | | | Overaged | | |
|---|---|---|---|---|---|---|
| | 7075-T651 | 7050-T6 | BAR-T6 | 7075-T7351 | 7050-T7352 | BAR-T7 |
| **Grain Boundary** | | | | | | |
| PFZ, $\mu$m | 0.070 | 0.050 | 0.060 | 0.083 | 0.085 | 0.095 |
| Mean Particle Diameter, D, $\mu$m | 0.032 | 0.046 ± 0.017 | 0.062 ± 0.032 | 0.094 ± 0.030 | 0.055 ± 0.020 | 0.086 ± 0.038 |
| Interparticle Spacing d, $\mu$m | 0.091 | 0.095 ± 0.010 | 0.118 ± 0.011 | 0.136 | 0.120 ± 0.020 | 0.137 ± 0.020 |
| d-D, $\mu$m | 0.059 | 0.049 | 0.056 | 0.038 | 0.065 | 0.051 |
| N, Particles/$\mu$m$^2$ | 120 | 112 ± 22 | 72 ± 13 | 55 | 70 ± 22 | 53 ± 16 |
| $A_f$, % | 9.6 | 18.6 | 21.7 | 38.1 | 16.6 | 30.8 |
| Large Particle Diameter, $\mu$m | 0.250 ± 0.090 | | | 0.505 ± 0.130 | | |
| **Matrix** | | | | | | |
| G.P. Zones, Å | spherical (75) | spherical (75) | spherical (75) | - | few spherical | - |
| $\eta'$, Å | ~ 5% (150) | 50% (~ 100) | 5% (~ 100) | 150-300 | 150 | 200 |
| $\eta$, Å | - | - | - | 400-800 | 250-550 | 600-1000 |
| Cr-Phase, $\mu$m | 0.1 | - | - | 0.1 | - | - |
| $MgZn_2$, $\mu$m | 0.2 | - | - | 0.2 | - | - |
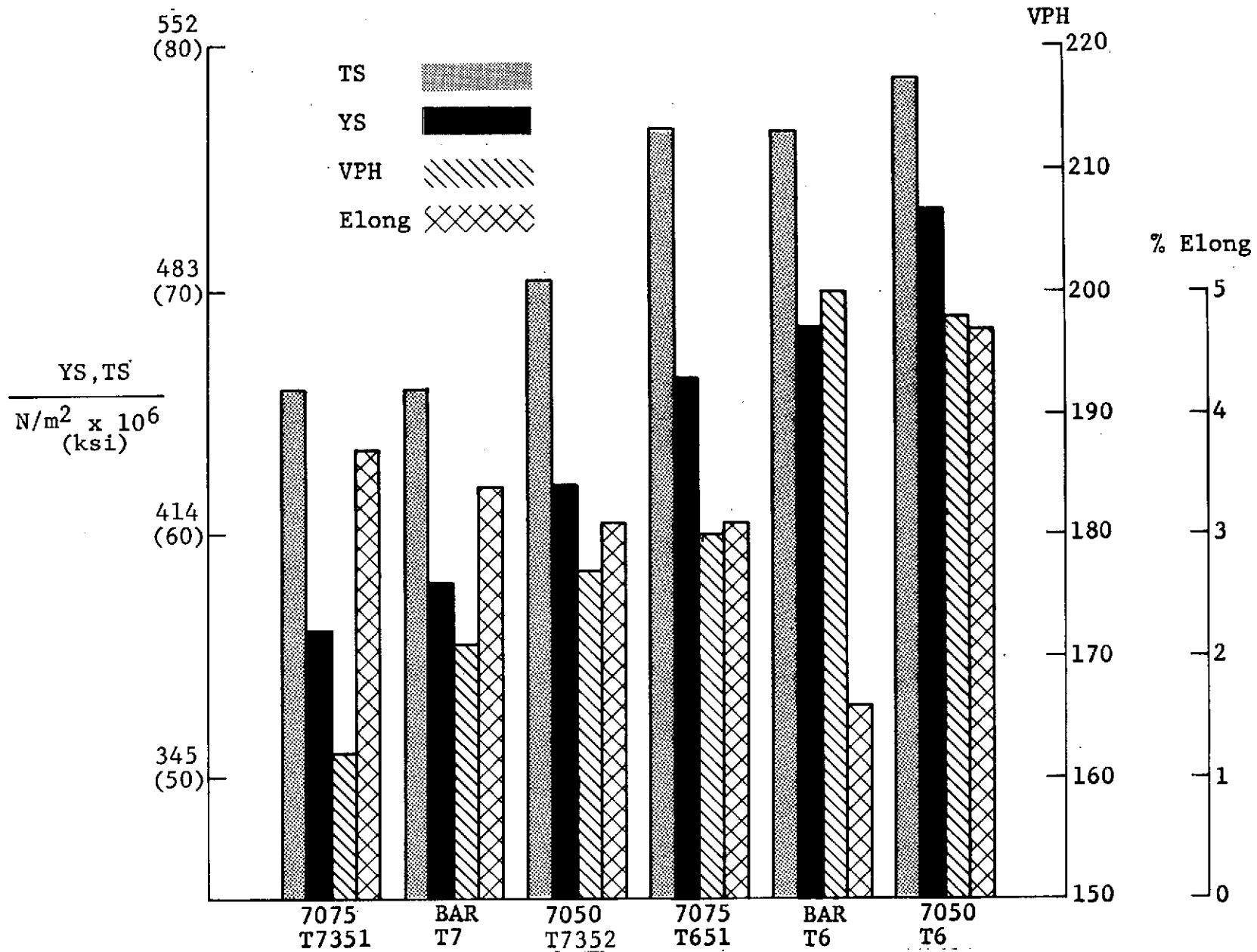
Fig. 1 Comparison of the Short Transverse Mechanical
Properties of 7075, BAR, and 7050 Aluminum Alloys
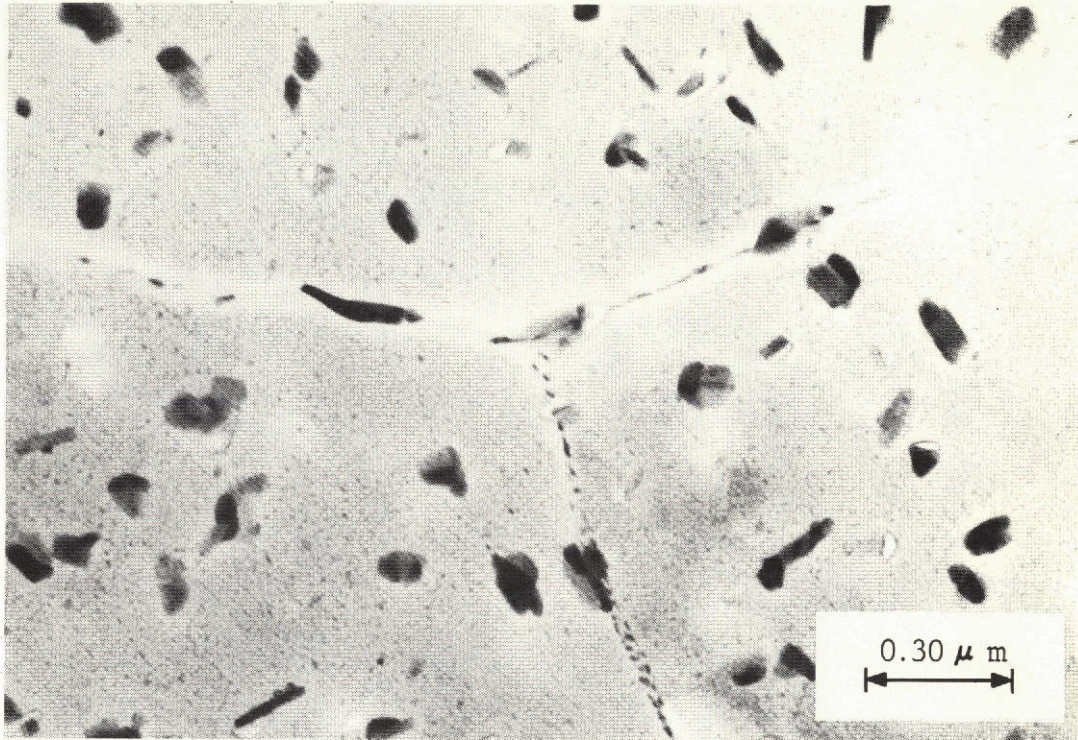
(a)
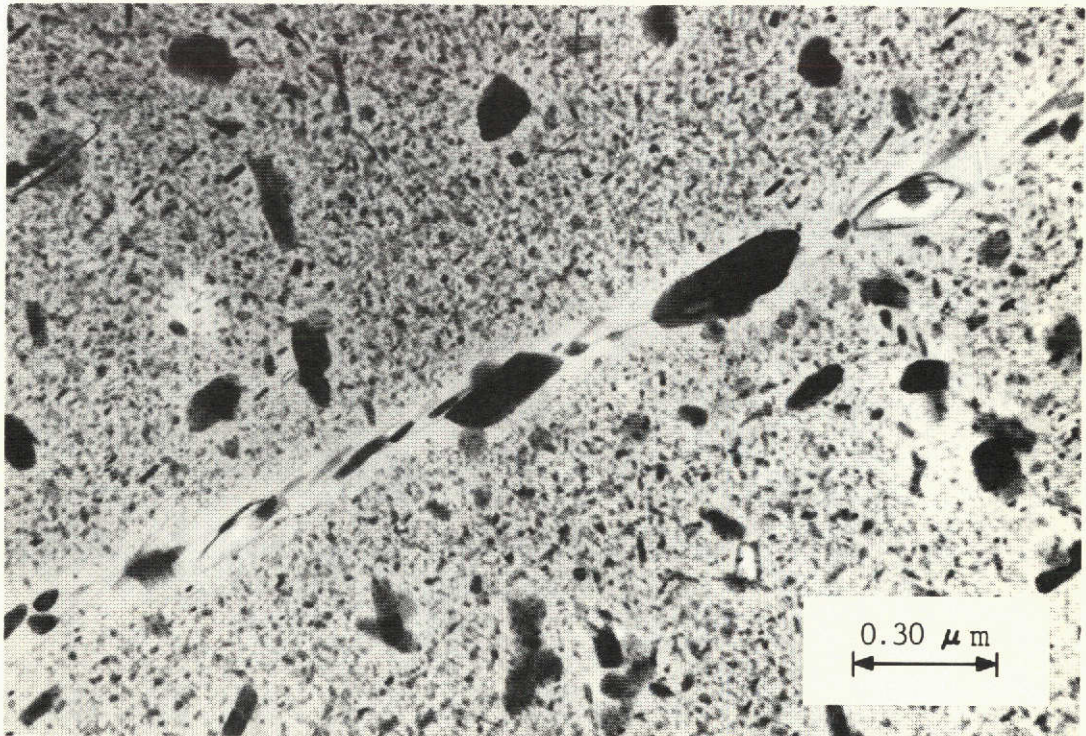


(b)

Fig. 2  Transmission Electron Micrographs of 7075 Aluminum Alloy:
(a) Highest Strength Temper, T651; (b) Overaged Temper,
T7351
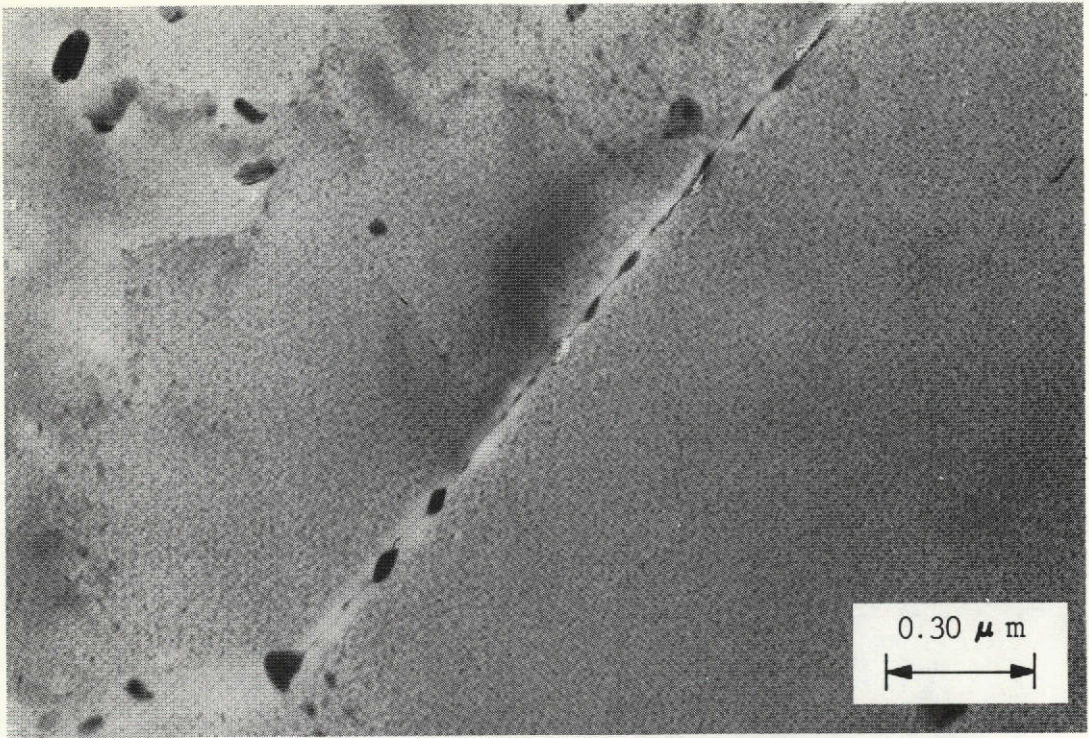
(a)
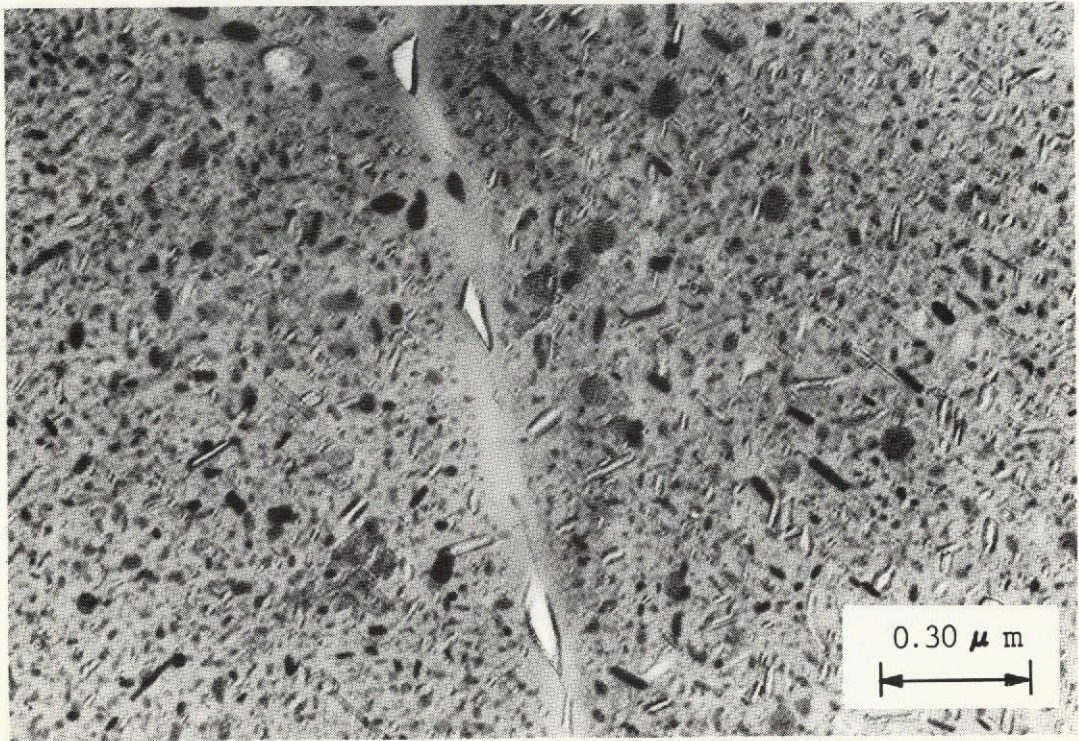


(b)

Fig. 3 Transmission Electron Micrographs of BAR Aluminum Alloy:
(a) Highest Strength Temper, T6; (b) the Overaged
Temper, T7

16
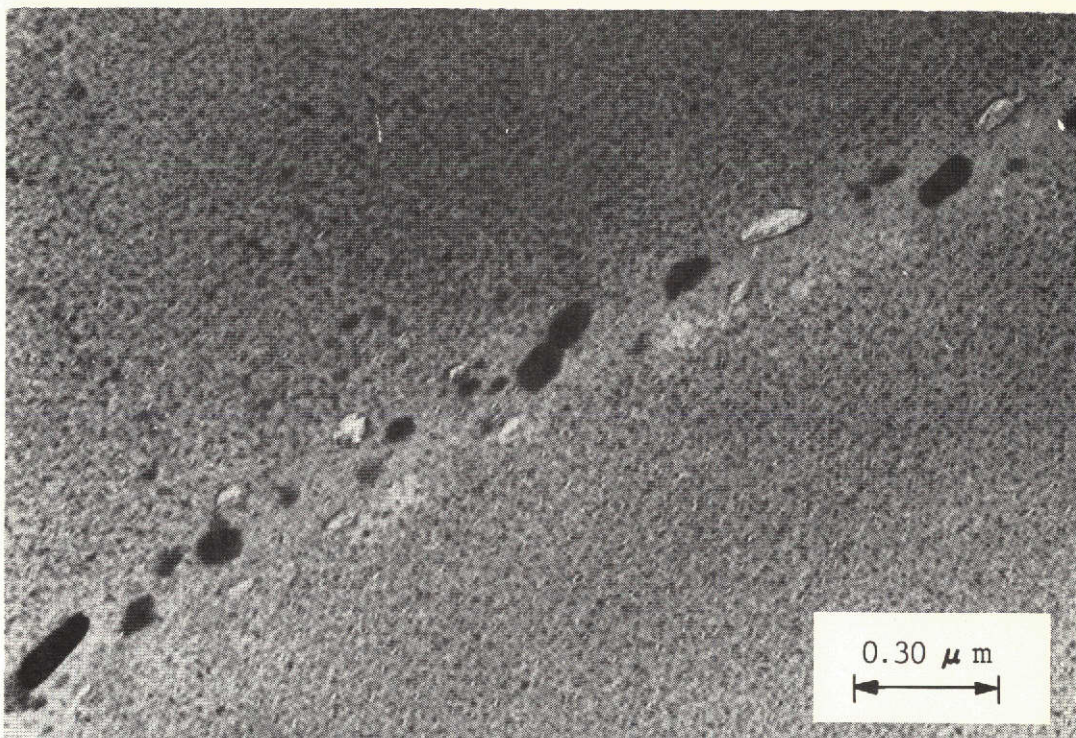
(a)
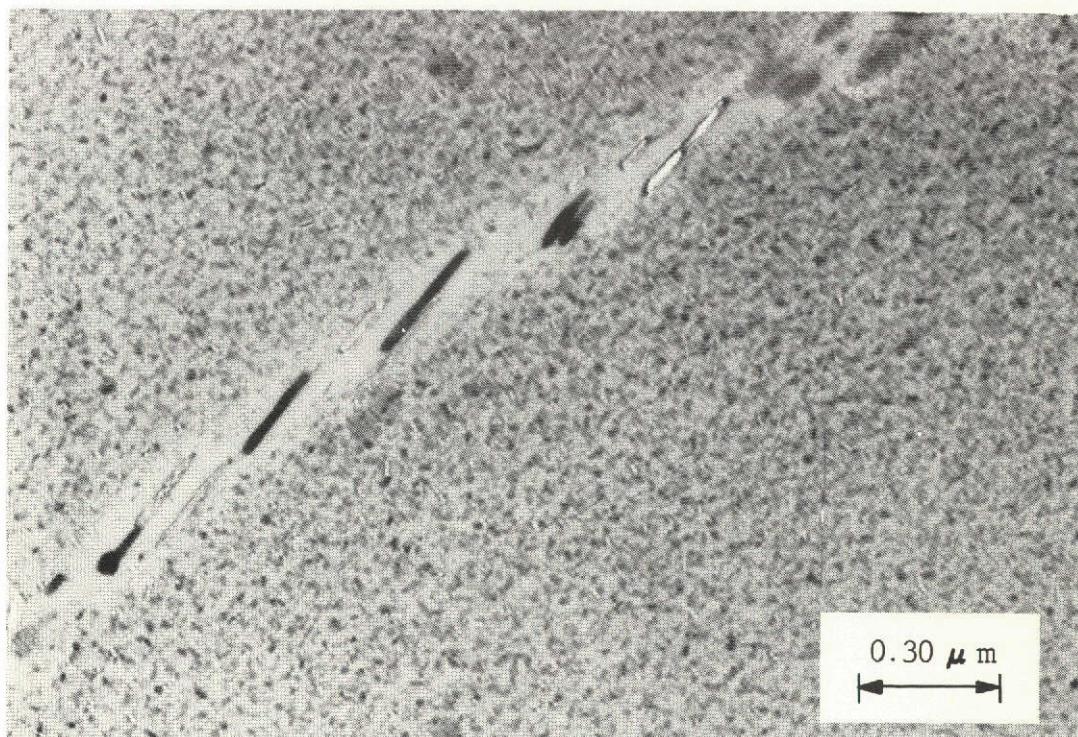


(b)

Fig. 4  Transmission Electron Micrographs of 7075 Aluminum
        Alloy: (a) Maximum Strength Temper, T6; (b) Overaged
        Temper, T7352

17

possibly some small incoherent η phase. The matrix of the overaged temper of the three alloys consists exclusively of η′ and η, but differences in the size and density of matrix precipitates can be seen. The 7050 alloy contains the smallest concentration of η, perhaps as little as 10 percent by volume; the 7075 alloy appears to contain approximately 30-40 percent; whereas the concentration of η in BAR is greater than 50 percent. In addition, the average size of η is approximately 400Å, 600Å, and 800Å in 7050, 7075, and BAR, respectively, as shown in Table 3.

Grain boundary microstructural characteristics are also listed in Table 3. The 7075 alloy is the only one that has a bimodal distribution of grain boundary precipitates. The grain boundary characteristics that are listed in Table 3 are:

PFZ — The total region on both sides of the grain boundary that is devoid of matrix precipitate

D — The average particle diameter

N — The particle density that was calculated based upon an average film thickness of 0.140μm

d — The average center-center interparticle spacing that was calculated from $1/N^2$

(d-D) — The mean edge-edge interparticle spacing

$A_f$ — Area fraction of grain boundary that is covered by precipitate

Based on our previous studies of the stress corrosion susceptibility of highest strength 7075, the most important microstructural characteristic affecting stress corrosion susceptibility is the average interparticle spacing, d (Ref. 5). Resistance to stress corrosion attack increases as the interparticle spacing increases. Parameters such as

18

PFZ width, matrix microstructure, area fraction covered, and particle size did not appear to affect the stress corrosion susceptibility in a systematic manner.

## C. Differential Scanning Calorimetry

The DSC technique was used to characterize the solid state reactions accompanying the formation and dissolution of precipitates for the six tempers described here. Typical results are shown in the differential specific heat, $\Delta C_p$, versus temperature curves in Figs. 5-7. In these figures, deviations from the horizontal are indicative of solid state reactions accompanying heating. The curves are based on calorimetric data that have been complemented by a temperature-dependent instrument calibration factor. The calibration factor was checked frequently using pure aluminum as a standard and was modified to correct for instrumental variations. To obtain the differential specific heat, i.e., the excess heat associated with reaction phenomena, a background specific heat term was used to account for the temperature-dependent specific heat of the aluminum rich solid solution and existing precipitates. The background specific heat was determined for each run by considering the initial and final measurements during which thermal equilibrium was approached as well as the measured specific heat over temperatures where no reaction takes place. For cases where reactions were indicated at the final measurement temperature, specifically for 7050-T7352, only the latter criteria could be used, and extrapolation of specific heat results was necessary. The background specific heat term was generally in fair agreement with that obtained by considering the Kopp-Neumann rule for the elemental constituency of these alloys (Ref. 58) and the temperature-dependent specific heat of pure aluminum.

Essentially, three regions are indicated in these figures:

- Region 1 - At lower temperatures there is an endothermic reaction indicative of the dissolution of the existing matrix precipitates (G.P. zones and/or $\eta'$ phase)
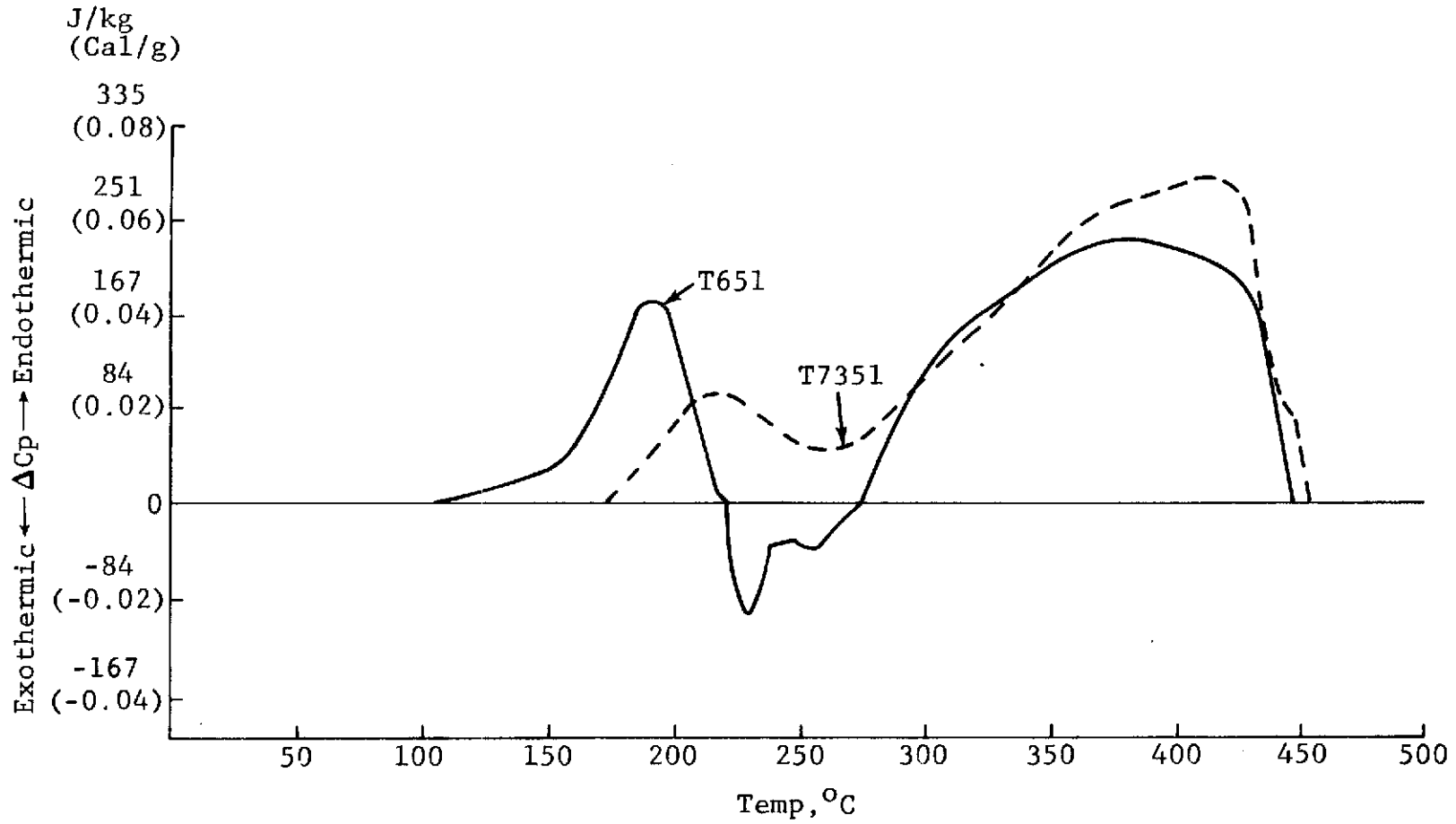
Fig. 5  Differential Scanning Calorimeter Results for 7075
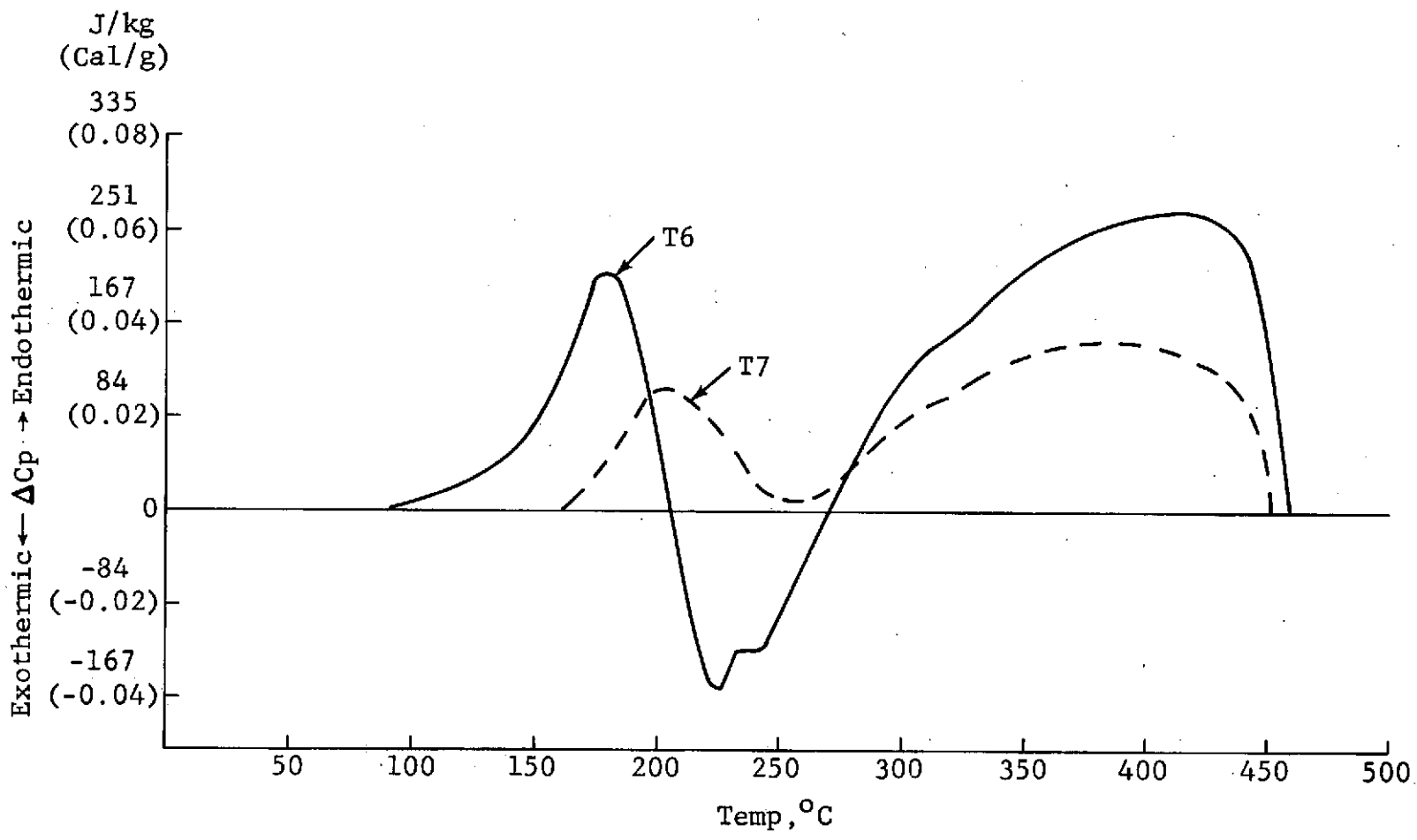Aluminum Alloy

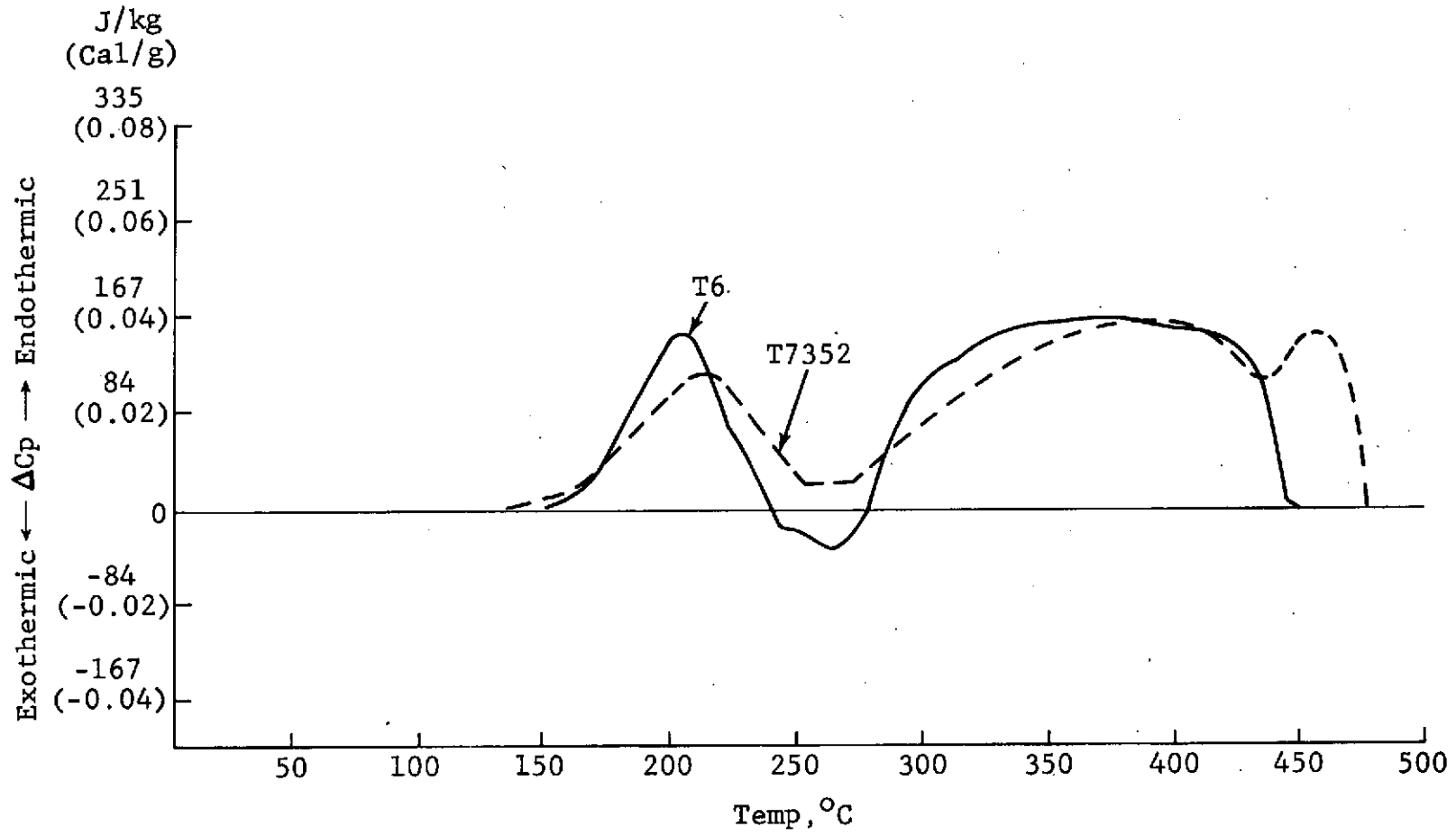Fig. 6  Differential Scanning Calorimeter Results for
BAR Aluminum Alloy

Fig. 7  Differential Scanning Calorimeter Results from 7050 Aluminum Alloy

- Region 2 - At intermediate temperatures there are exothermic reactions indicative of the formation of $\eta'$ and $\eta$ phases. This region is absent for the overaged tempers

- Region 3 - At temperatures above 285°C, there is an endothermic reaction region associated with the dissolution of $\eta$ phase

In this work, we have focused our attention on Region 1, since it relates to the existing microstructural features significant to strengthening, i.e., G.P. zones and $\eta'$ phase. The matrix precipitate structures for these tempers have previously been described and are listed in Table 3 and shown in Figs. 2-4.

The peak dissolution temperature in Region 1 is an indicator of the stability of existing precipitates. These temperatures are listed in Table 4. For each of the alloys, the overaged temper has the higher peak temperature and would have greater thermal stability than the highest strength temper. However, the difference in peak temperature between highest strength and overaged tempers is 29°C for 7075 and BAR, whereas it is only 5°C for 7050.

TABLE 4  MATRIX PRECIPITATE DISSOLUTION CHARACTERISTICS

| Material | Peak Temp. °C | $\Delta H_D$ | | $\Delta H^{\ddagger}$ | | $\Delta S^{\ddagger}$ | |
|---|---|---|---|---|---|---|---|
| | | J/kg | cal/g | kJ/mol | kcal/mol | kJ/mol °K | eu |
| 7075-T651 | 189 | 6740 | 1.61 | 101.7 | 24.3 | - 86.2 | -20.6 |
| 7075-T7351 | 218 | 6230 | 1.49 | 83.7 | 20.0 | -141.0 | -33.7 |
| BAR-T6 | 181 | 8280 | 1.98 | 89.1 | 21.3 | -109.6 | -26.2 |
| BAR-T7 | 210 | 5980 | 1.43 | 82.4 | 19.7 | -138.9 | -33.2 |
| 7050-T6 | 200 | 5980 | 1.43 | 107.5 | 25.7 | - 80.8 | -19.3 |
| 7050-T7352 | 205 | 5650 | 1.35 | 84.1 | 20.1 | -131.4 | -31.4 |

The area under the $\Delta C_p$ versus temperature curve of Region 1 is a measure of the heat of reaction associated with precipitate dissolution. This heat, $\Delta H_D$, represents the product of the number of precipitates undergoing dissolution per gram of sample and their average heat of dissolution. Values of $\Delta H_D$ for all the tempers are also indicated in Table 4. For the three alloys, $\Delta H_D$ is higher for the highest strength temper. The higher dissolution energy is associated with the presence of G.P. zones. However, the dissolution energy for the highest strength temper of 7050 is comparable to that of the overaged tempers of the 7075 and BAR alloys. This is most unusual since the 7050-T6 temper has the highest strength of all the tempers examined (see Fig. 1). This anomaly suggests that the precipitate structure contributing to strengthening in 7050-T6 is different than that in other highest strength tempers. In addition the higher peak temperature for this temper, 200°C as opposed to 181 and 189°C for BAR-T6 and 7075-T651, respectively, is consistent with the transmission electron microscopy evaluation that shows a much higher concentration of $\eta'$ in the matrix of 7050-T6. The low value of $\Delta H_D$ appears to be related to the comparatively low concentration of G.P. zones in the matrix of this temper.

The $\Delta C_p$ versus temperature curves in Figs. 5-7 are also used to evaluate the kinetics associated with the indicated reactions (Ref. 57). This has been done for Region 1, and we have applied absolute reaction rate theory (Ref. 59) to study this dissolution reaction for each temper under consideration. The activation enthalpy, $\Delta H^{\ddagger}$, and activation entropy, $\Delta S^{\ddagger}$, have been calculated utilizing computer-assisted analysis; these values are given in Table 4. For the three overaged tempers, $\Delta H^{\ddagger}$ and $\Delta S^{\ddagger}$ are quite similar. For the highest strength tempers, $\Delta H^{\ddagger}$ and $\Delta S^{\ddagger}$ are consistently higher and lower, respectively, than those of the overaged tempers. The results for 7050-T6, however, are unusual since the matrix precipitate undergoing dissolution is somewhat intermediate between the predominant G.P. zone matrix of BAR-T6 and 7075-T651 and the $\eta' + \eta$ matrix of the overaged tempers. An intermediate activation enthalpy and entropy would have been expected; instead, 7050-T6 has the highest activation enthalpy and lowest activation entropy of all the tempers studied.

## D. Optical Microscopy

The grain morphology of 7050 and BAR alloys was evaluated since the susceptibility of 7075-T651 to stress corrosion attack was found to be dependent on grain anisotropy (Ref. 9). Representative photomicrographs of the overaged temper for the three alloys of interest are shown in Fig. 8. The average grain size in the short transverse direction, $d_{\|}$, the long transverse direction, $d_{\perp}$, and the anisotropy factor, $d_{\perp}/d_{\|}$, are listed in Table 5. These values were

TABLE 5   GRAIN MORPHOLOGY OF
7075, 7050, AND BAR ALLOYS

| Alloy | Grain Size | | Anisotropy Factor $(d_{\perp}/d_{\|})$ |
|---|---|---|---|
| | $d_{\|}$, μm | $d_{\perp}$, μm | |
| 7075 | 95 ± 6 | 157 ± 46 | 1.7 |
| 7050 | 6.4 ± 0.8 | 7.8 ± 1.2 | 1.2 |
| BAR | 4.6 ± 0.6 | 8.3 ± 1.4 | 1.8 |

determined using the intercept method (Ref. 60), and the designations represent directions parallel and perpendicular to the direction of loading in mechanical and stress corrosion testing. It is apparent that gross differences in grain size exist between 7075 and the recently developed BAR and 7050 alloys, with the 7075 having almost a 20× larger grain size than the other two.

## E. Stress Corrosion

Stress corrosion test results for highest strength and overaged tempers of 7050, BAR, and 7075 aluminum alloys are shown in Figs. 9-23. The time-to-failure (TTF), time for cracking to initiate in smooth surface specimens $(t_{inc})$, and time for cracks to propagate $(t_p)$ are illustrated over a pH range from 0.7 to 3.4. Results for 7075 were

obtained previously (Refs. 5 and 36) and are shown for comparison.

The TTF can be regarded as a measure of the overall susceptibility of a specimen to stress corrosion attack. The TTF results in the highest strength and overaged tempers of 7075, BAR, and 7050 aluminum alloys are shown in Figs. 9-11, respectively. Each data point in these and subsequent figures represents the average of at least two stress corrosion tests. The error bars indicate the maximum and minimum values at a designated pH. For 7075 and BAR (Figs. 9 and 10) the relative behavior between tempers is as expected; i.e., the highest strength temper is more susceptible than the overaged temper. On the other hand, the highest strength temper of 7050-T6 is more resistant to stress corrosion attack than the overaged T7352 temper, as shown in Fig. 11. This unusual reversal in the behavior of 7050 may not exist at higher pH. A crossover between the T6 and T7352 curves could occur at higher pH, but this is not apparent from the present results. Testing over the 3 to 7 pH range would help to clarify the overall behavior of these tempers.

Comparison of TTF results of 7075, BAR, and 7050 in the highest strength and overaged tempers is made in Figs. 12 and 13, respectively. At lower pH, the curves all have an approximate linear region. In the case of the highest strength temper, this linear region extends to approximately pH 1.5, 2.0, and 2.5 for 7050, 7075, and BAR, respectively; whereas for the overaged temper, the linear portion of the curve ends at approximately pH 2.0, 1.5, and 2.0 for 7050, 7075, and BAR, respectively. In this low pH region, the slope for the highest strength tempers of 7050 and 7075 is approximately equal; but that for BAR is approximately 40 to 50 percent less than that for the other two. For the overaged temper, the slope of the lower pH portion of the 7075 curve is approximately 50 percent larger than that for 7050 and BAR. To account for the approximately linear behavior in this region, a pH dependent mechanism of attack, probably dissolution controlled, has been suggested (Ref. 36).

At higher pH, above 2.0-2.5, most of the TTF versus pH curves in Figs. 12 and 13 become relatively flat, and only slight pH dependence is indicated. This change in

26

slope at higher pH suggests that a different mechanism of attack becomes rate controlling. Sufficient time was not available to obtain data to pH 3.4 for all tempers examined. Results at higher pH would help to characterize the stress corrosion susceptibility of these tempers.

Our method of testing enables separation of the contribution of initiation and propagation stages to the overall TTF. Comparison of crack propagation times, $t_p$, for .the highest strength and overaged tempers for 7075, BAR, and 7050 are shown in Figs. 14-16, respectively. For each alloy, $t_p$ for the overaged temper is greater than that for the corresponding highest strength temper, and similar pH dependence is indicated. The difference in $t_p$ between highest strength and overaged tempers is greatest for 7075 and smallest for 7050.

Comparison of the crack propagation times of these alloys in their highest strength and overaged tempers is shown in Figs. 17 and 18, respectively. These results also indicate an approximately linear region at lower pH. The crack propagation time for 7075 at pH = 2.5 is much greater than that for BAR and 7050 in both the highest strength and overaged temper comparisons.

We have defined the time required to initiate cracking in a smooth surface specimen as the crack incubation time, $t_{inc}$. Comparisons between $t_{inc}$ for the highest strength and overaged tempers of 7075, BAR, and 7050 are illustrated in Figs. 19-21, respectively. For the overaged temper of 7075, $t_{inc}$ appears to be pH independent at about pH 2.5, whereas for the highest strength temper, $t_{inc}$ continues to exhibit a pH dependent increase at pH 3.0. Extrapolation of these curves to higher pH would indicate a crossover at pH $\simeq$ 3.5. The incubation time results for BAR are similar to those for 7075. The overaged temper is more resistant to crack initiation than the highest strength temper at lower pH, but appears slightly more susceptible at higher pH. On the other hand, the highest strength temper of 7050 is much more resistant to crack initiation than the overaged temper over the pH range studied. This large difference in $t_{inc}$ accounts for the higher overall resistance of the T6 temper to stress corrosion attack at pH $\leq$ 2.5 (see Fig. 11).

The effect of pH on $t_{inc}$ for the highest strength and overaged tempers of 7075, BAR, and 7050 is shown in Figs. 22 and 23, respectively. The overaged tempers have comparable incubation times at all pH levels, whereas large differences in $t_{inc}$ are observed between 7050-T6 on the one hand and 7075-T651 and BAR-T6 on the other. At pH 2.5 the time to initiate cracking for the highest strength temper of 7050 is approximately two orders of magnitude greater than that for either 7075 or BAR. Although the propagation time for 7075-T651 is greater than that of 7050-T6, the extremely long incubation time of 7050-T6 accounts for its superior overall stress corrosion resistance (see Fig. 12). This emphasizes the fact that a detailed understanding of the factors affecting the overall susceptibility can only be obtained if the separate stages are individually analyzed.

Alternate immersion stress corrosion testing in synthetic seawater (pH = 8.2) and 3.5 percent NaCl solution (pH 6.8-7.2) was also performed on the highest strength and overaged tempers of 7075, BAR, and 7050. Data for an initial stress level of $172 \times 10^6$ and $310 \times 10^6 N/m^2$ (25 ksi and 45 ksi) are shown in Fig. 24. Although these data are not as detailed as that generated at pH $< 3.4$, comparisons can be drawn. For the highest strength temper at $172 \times 10^6 N/m^2$ (25 ksi), 7050 is more resistant to attack than either BAR or 7075. For the overaged temper at both $172 \times 10^6$ and $310 \times 10^6 N/m^2$ (25 and 45 ksi), 7075 and 7050 are far more resistant to attack than BAR. The overaged 7075 appears most resistant to attack in the synthetic seawater environment, and the overaged 7050 is slightly more resistant to attack than 7075 in a 3.5 percent NaCl solution at $310 \times 10^6 N/m^2$ (45 ksi).
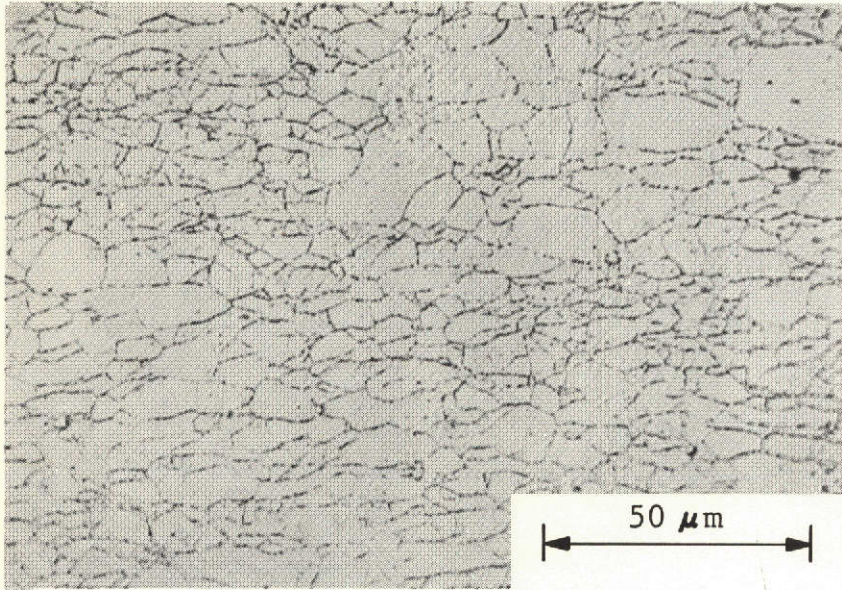
(a) BAR
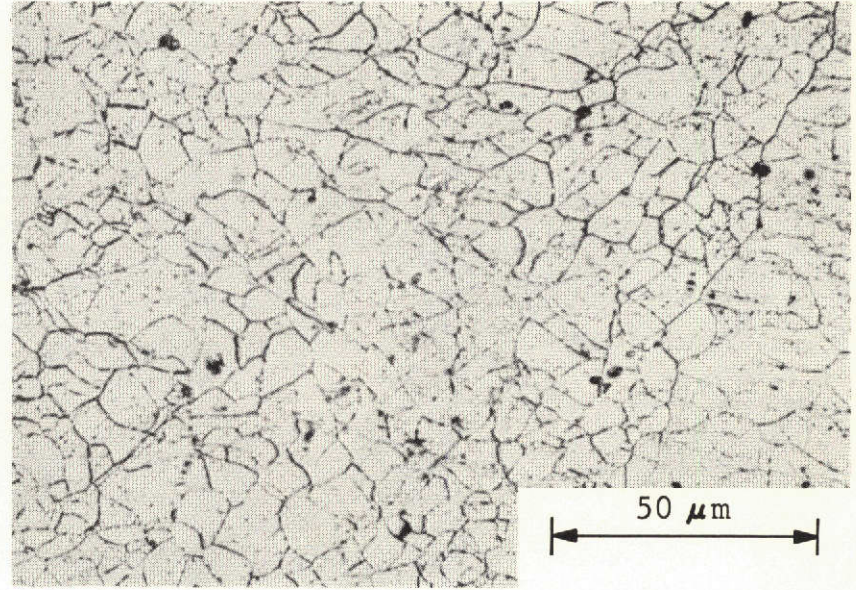
(b) 7050
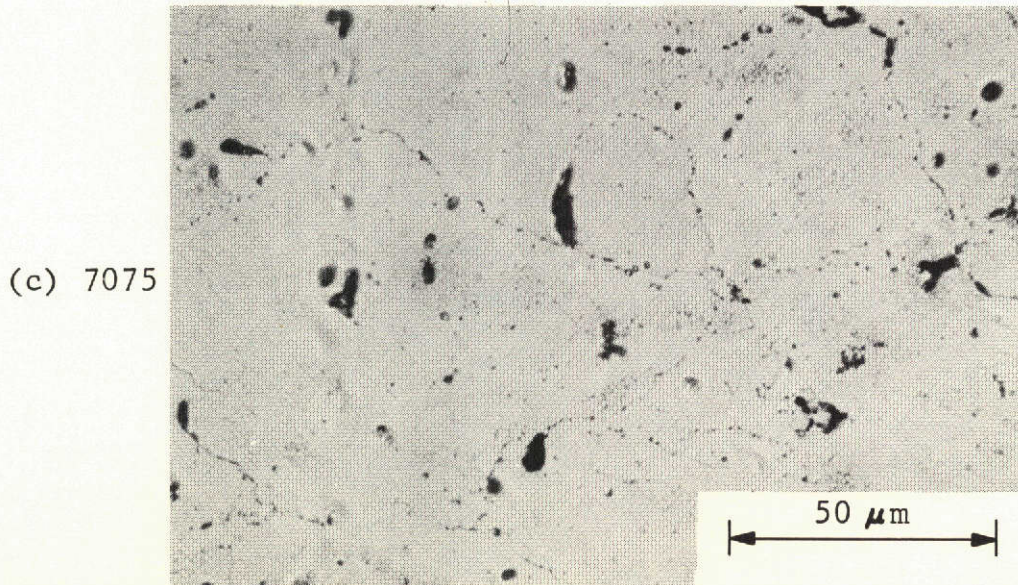
(c) 7075

Fig. 8  Photomicrographs of the Overaged Temper of BAR, 7050, and 7075 Aluminum Alloys.  The short and long transverse directions are vertical and horizontal, respectively.

Fig. 9   Effect of pH on Time-to-Failure of Highest Strength
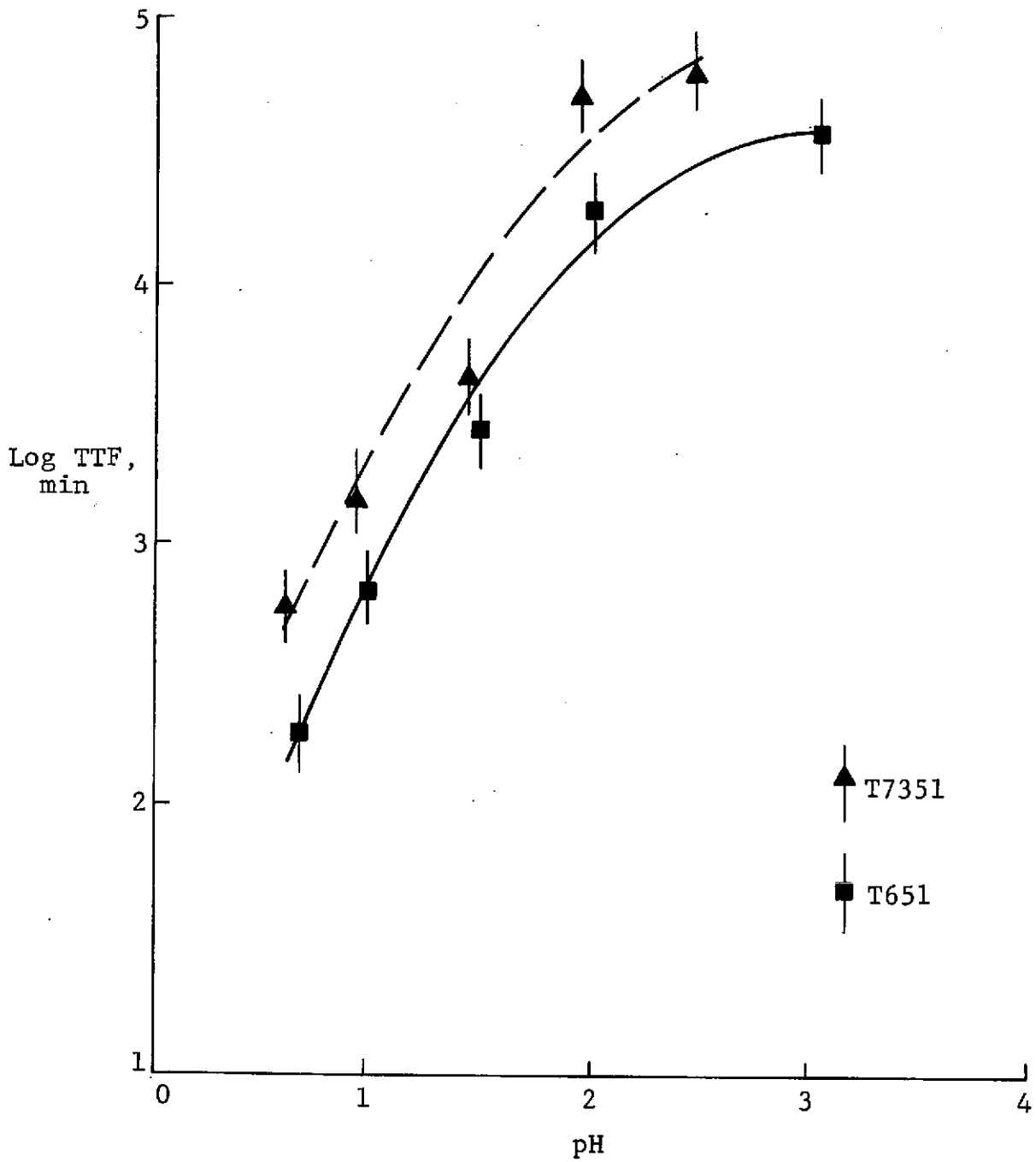and Overaged 7075 Aluminum Alloy

30
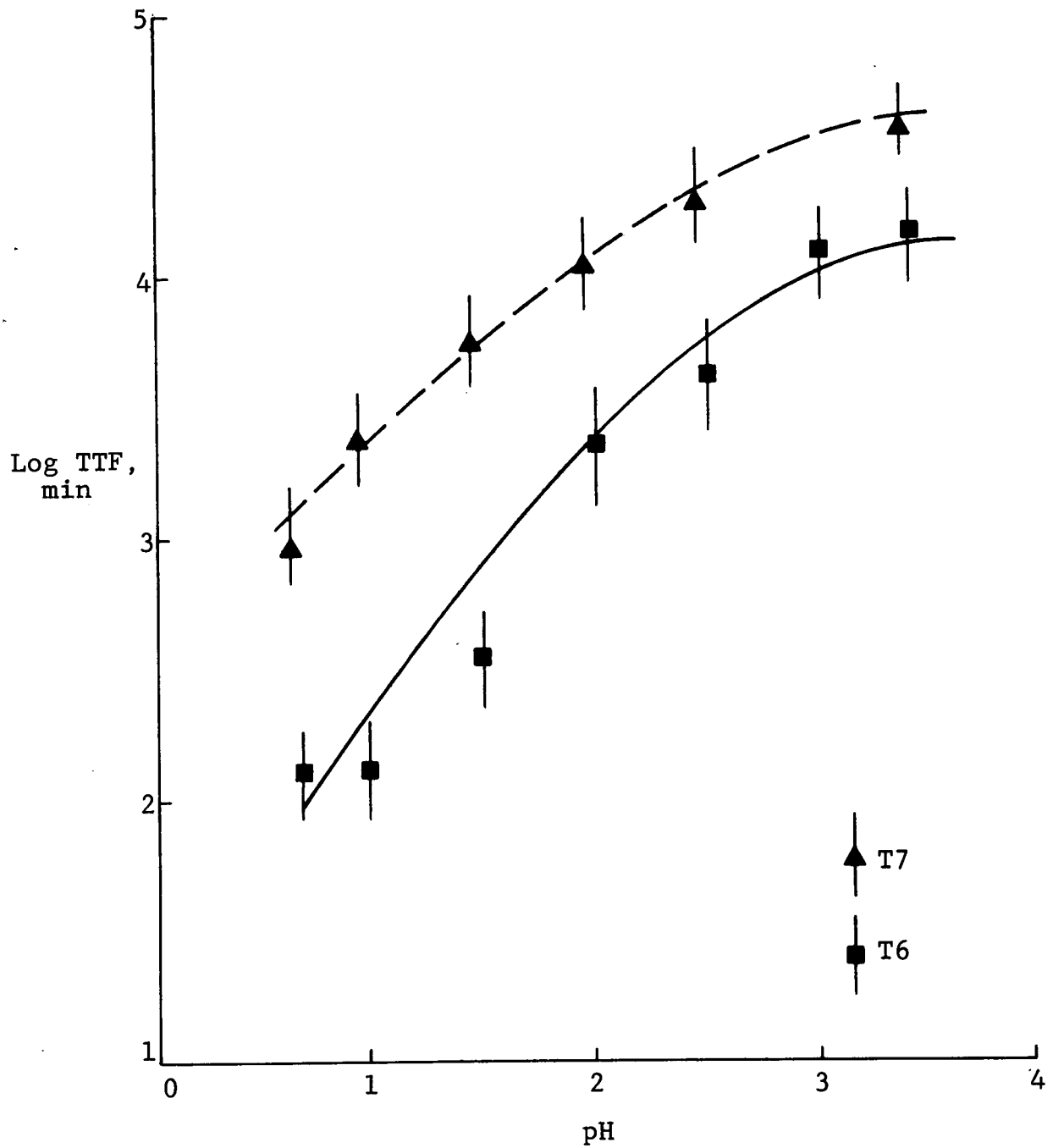
Fig. 10   Effect of pH on Time-to-Failure of Highest Strength
and Overaged BAR Aluminum Alloy

31

Fig. 11   Effect of pH on Time-to-Failure of Highest Strength
and Overaged 7050 Aluminum Alloy

32

Fig. 12   Comparison of the Time-To-Failure of the Highest Strength
          Tempers of 7075, BAR, and 7050 Aluminum Alloys

33

Fig. 13  Comparison of the Time-to-Failure for the Overaged
Tempers of 7075, BAR, and 7050 Aluminum Alloys
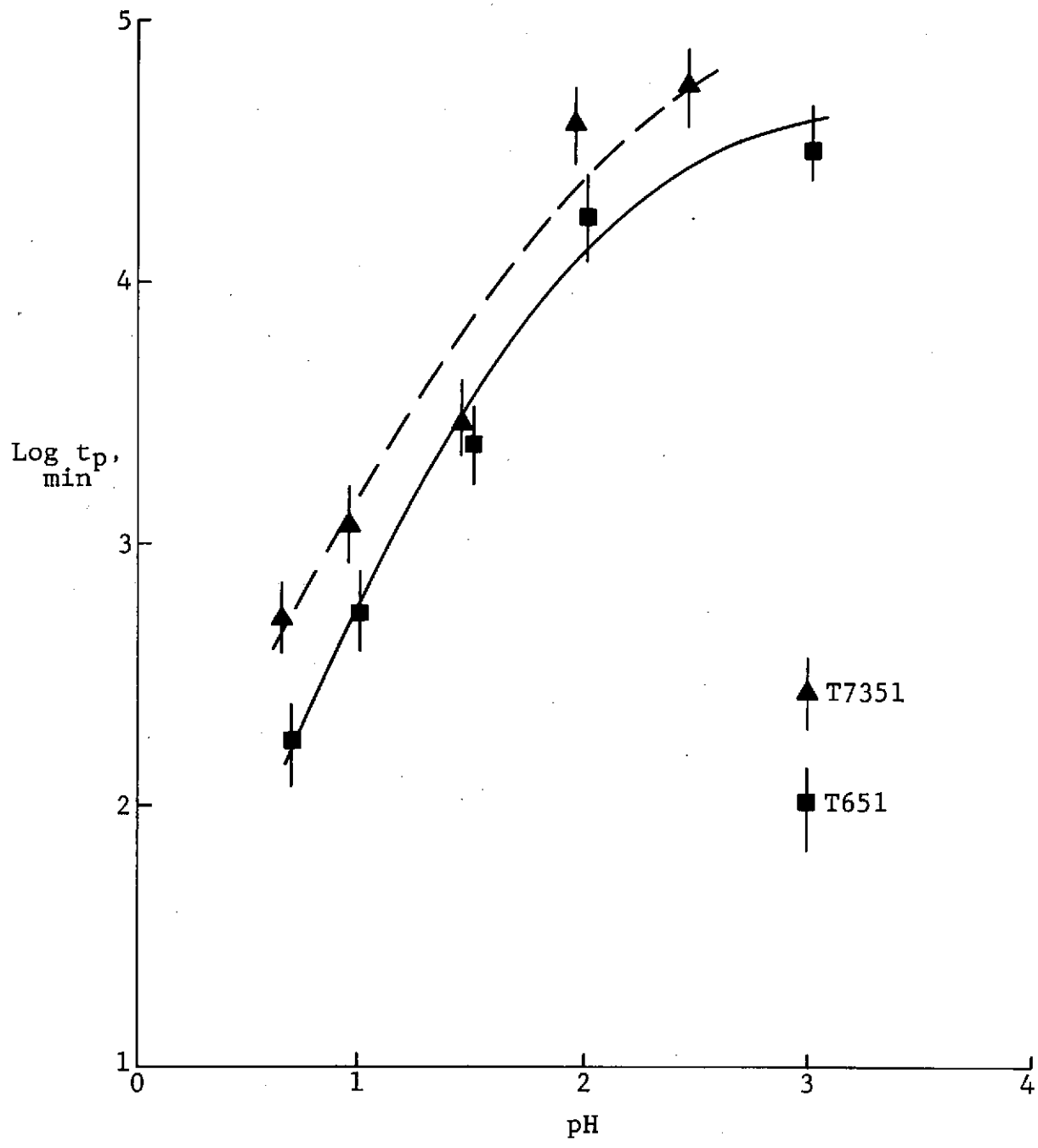
Fig. 14   Effect of pH on the Crack Propagation Time of Highest
Strength and Overaged 7075 Aluminum Alloy
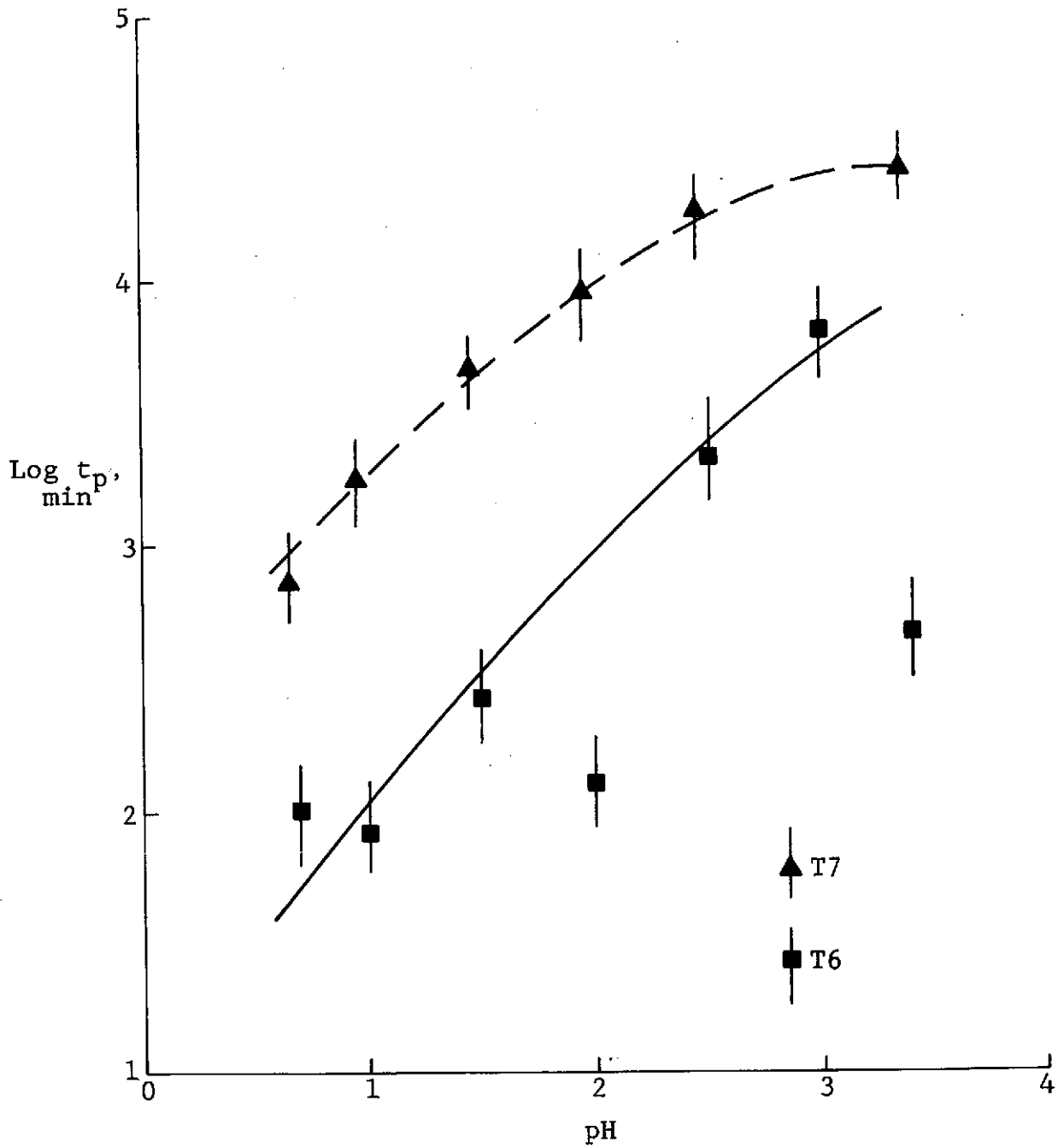
Fig. 15  Effect of pH on the Crack Propagation Time of Highest
Strength and Overaged BAR Aluminum Alloy
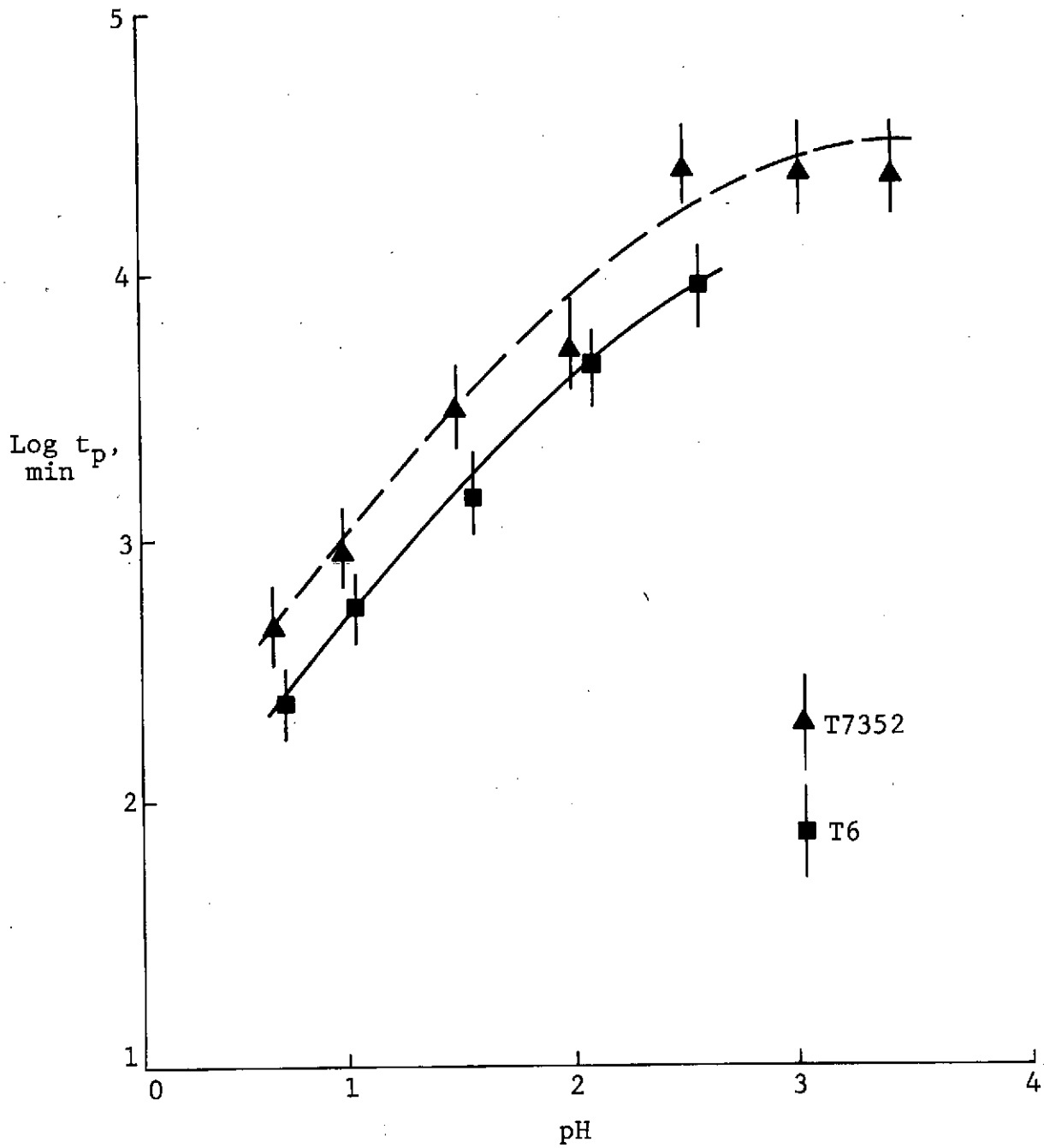
Fig. 16    Effect of pH on the Crack Propagation Time of
          Highest Strength and Overaged 7050 Aluminum Alloy
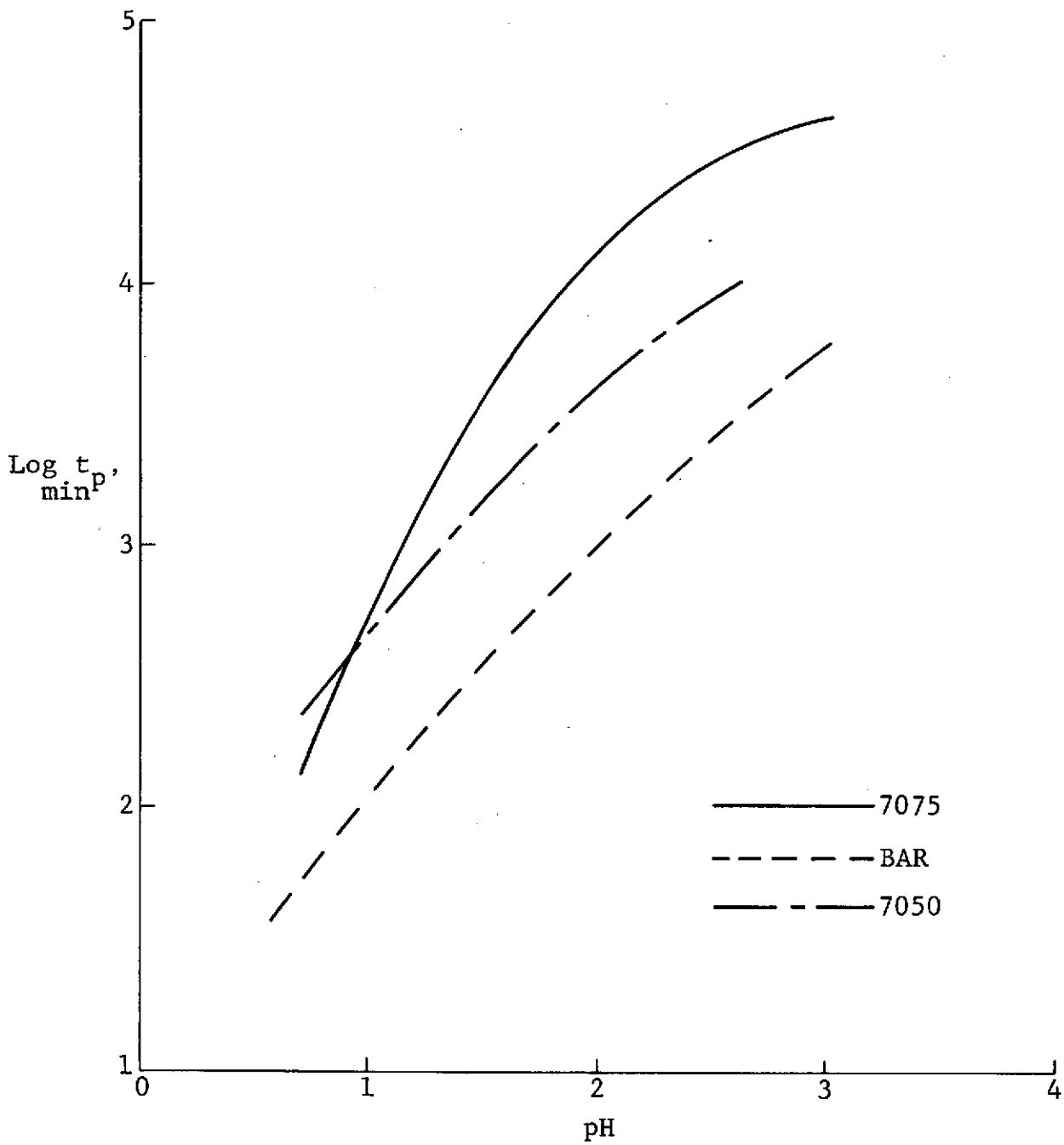
Fig. 17    Comparison of the Crack Propagation Time for the
           Highest Strength Tempers of 7075, BAR, and 7050
           Aluminum Alloys
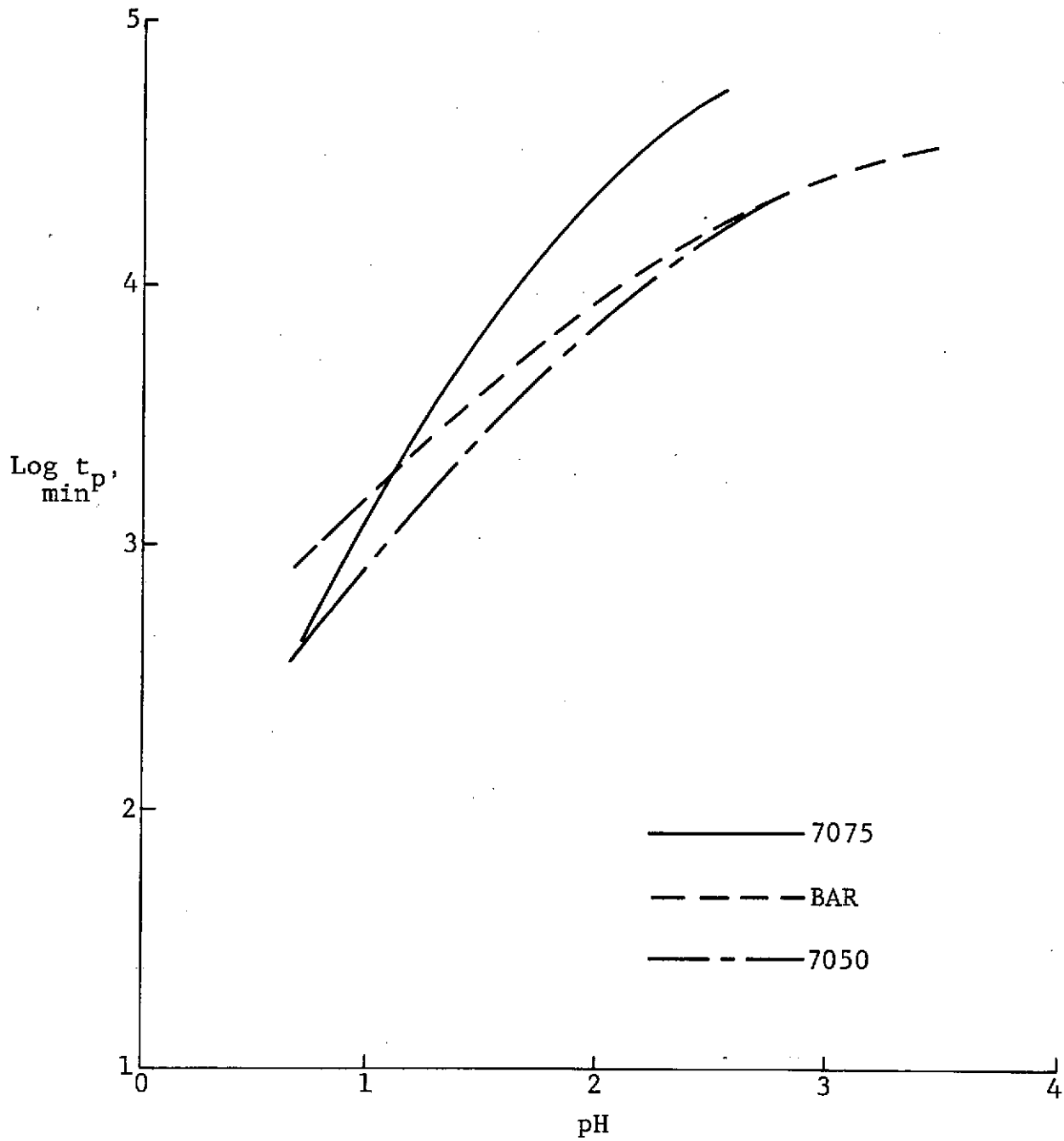
Fig. 18  Comparison of the Crack Propagation Time for the Over-
aged Tempers of 7075, BAR, and 7050 Aluminum Alloys
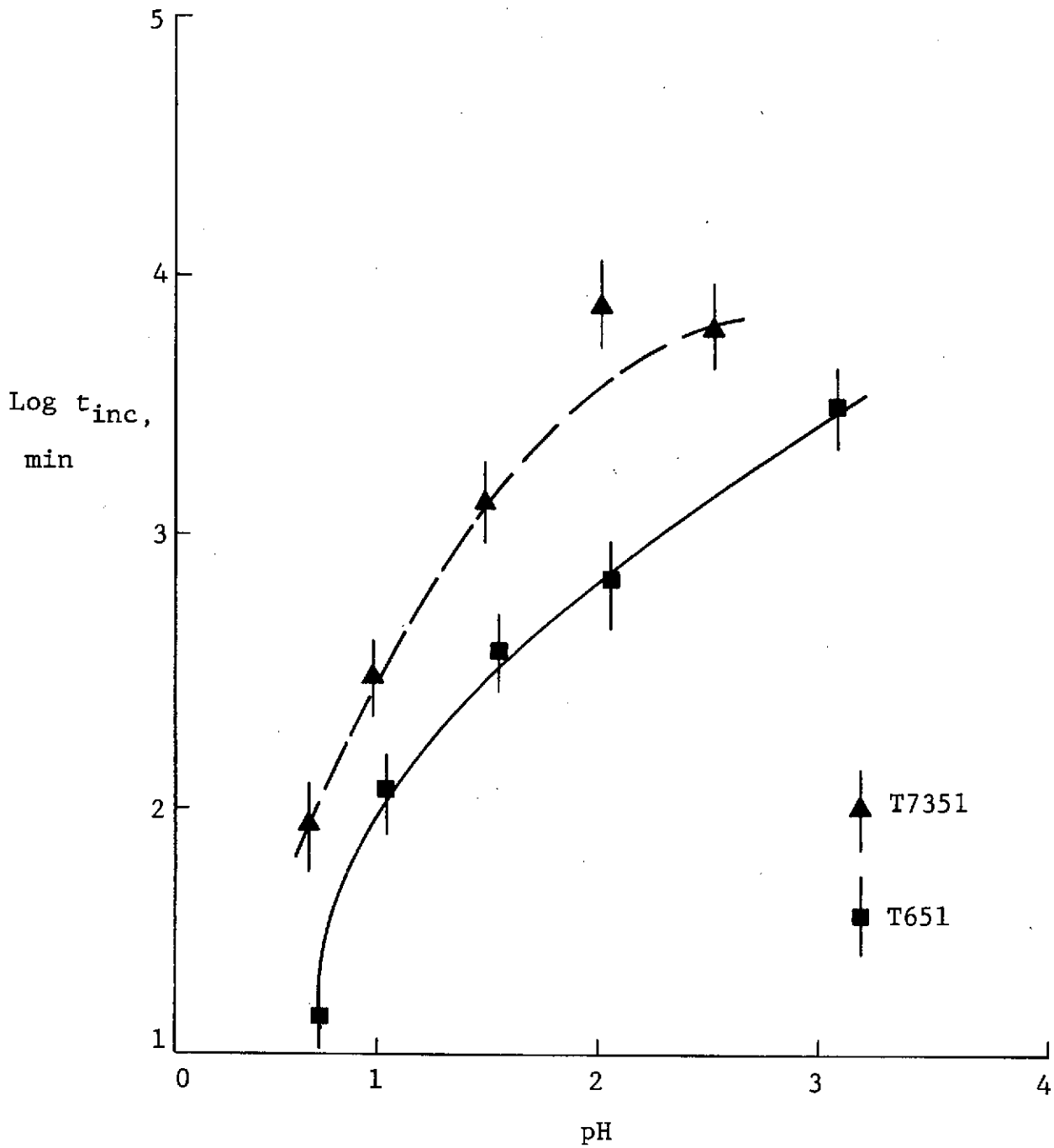
Fig. 19 Effect of pH on the Crack Initiation Time of Highest Strength and Overaged 7075 Aluminum Alloy
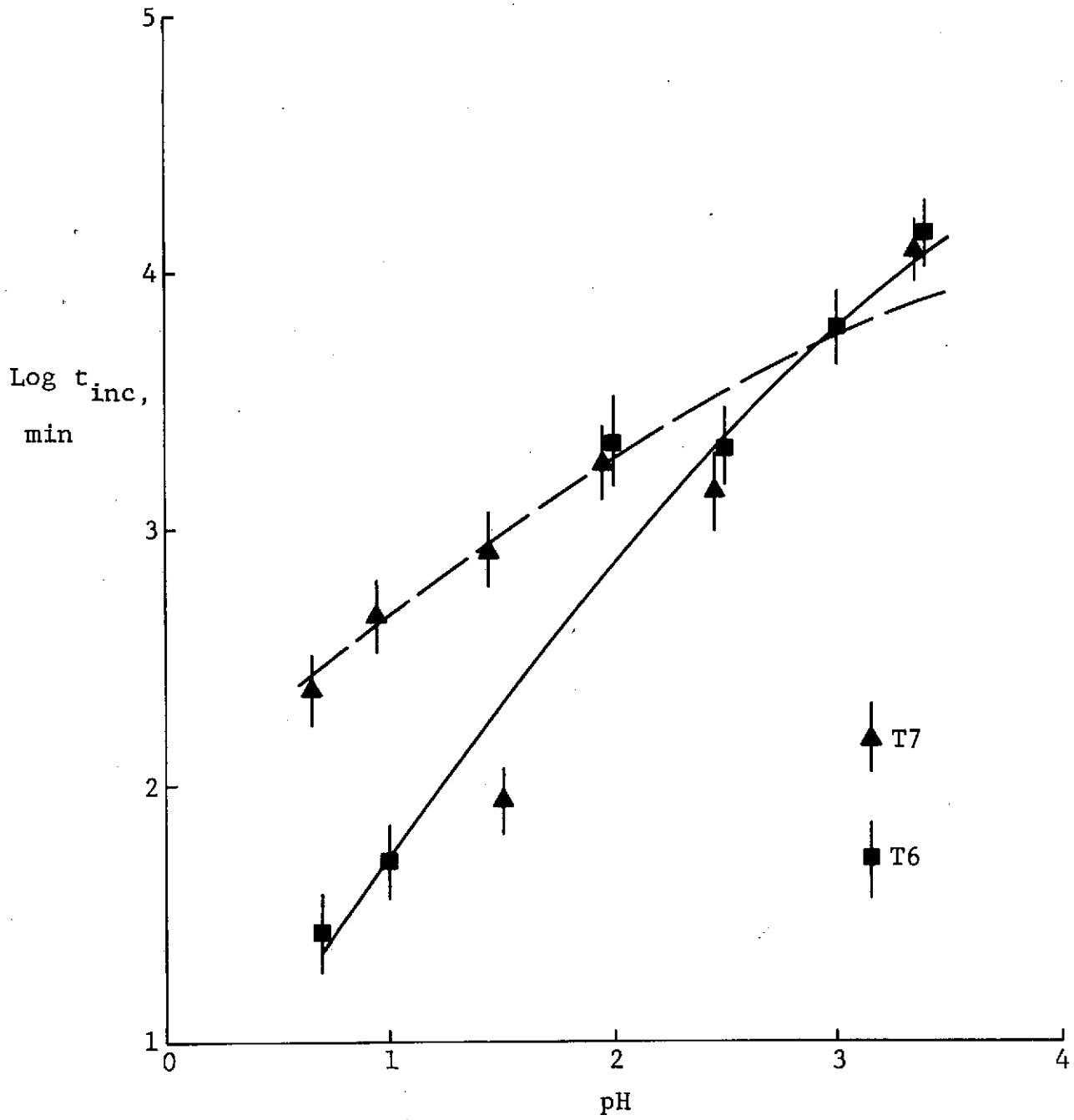
Fig. 20   Effect of pH on the Crack Initiation Time of
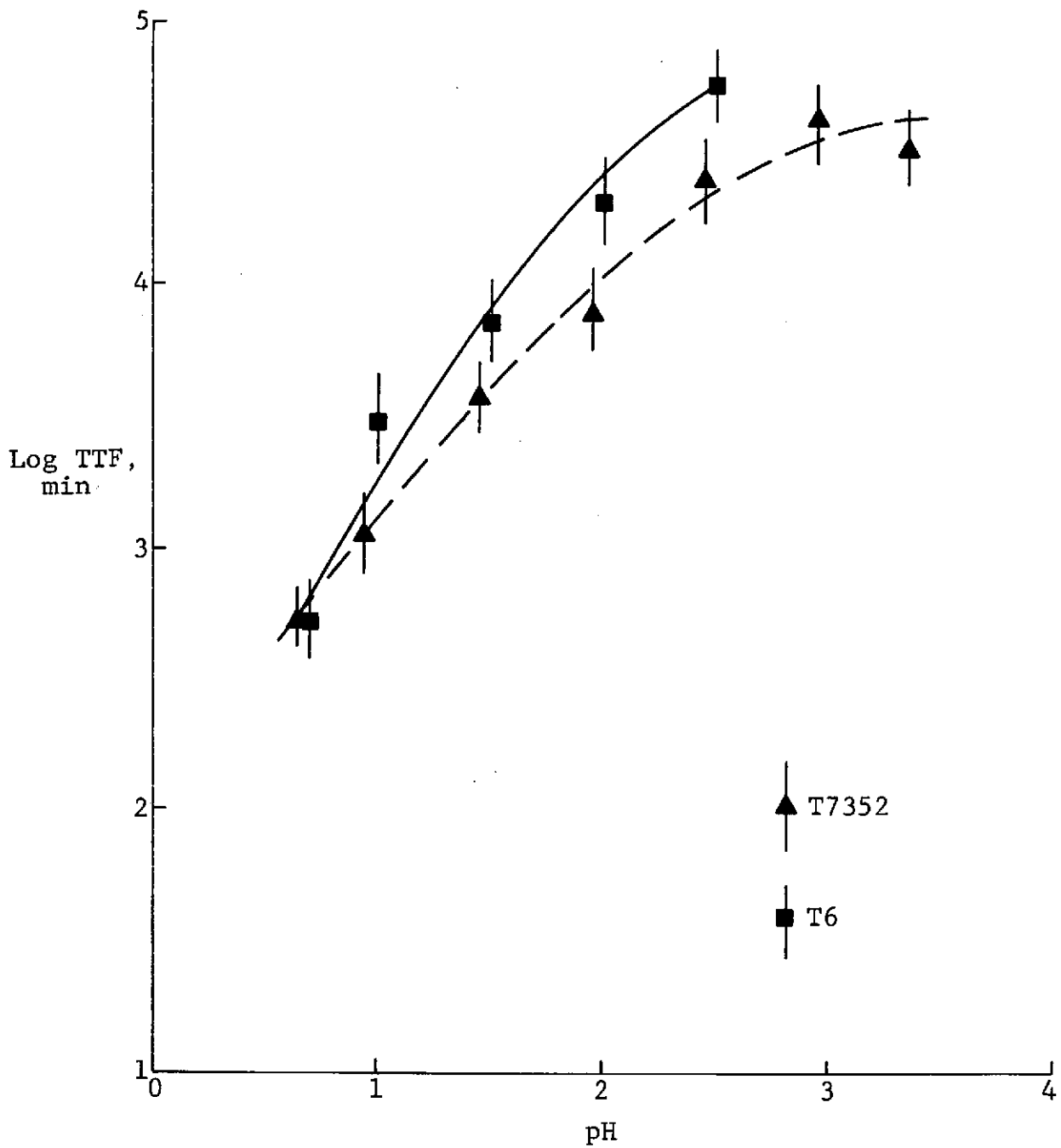Highest Strength and Overaged BAR Aluminum
Alloy
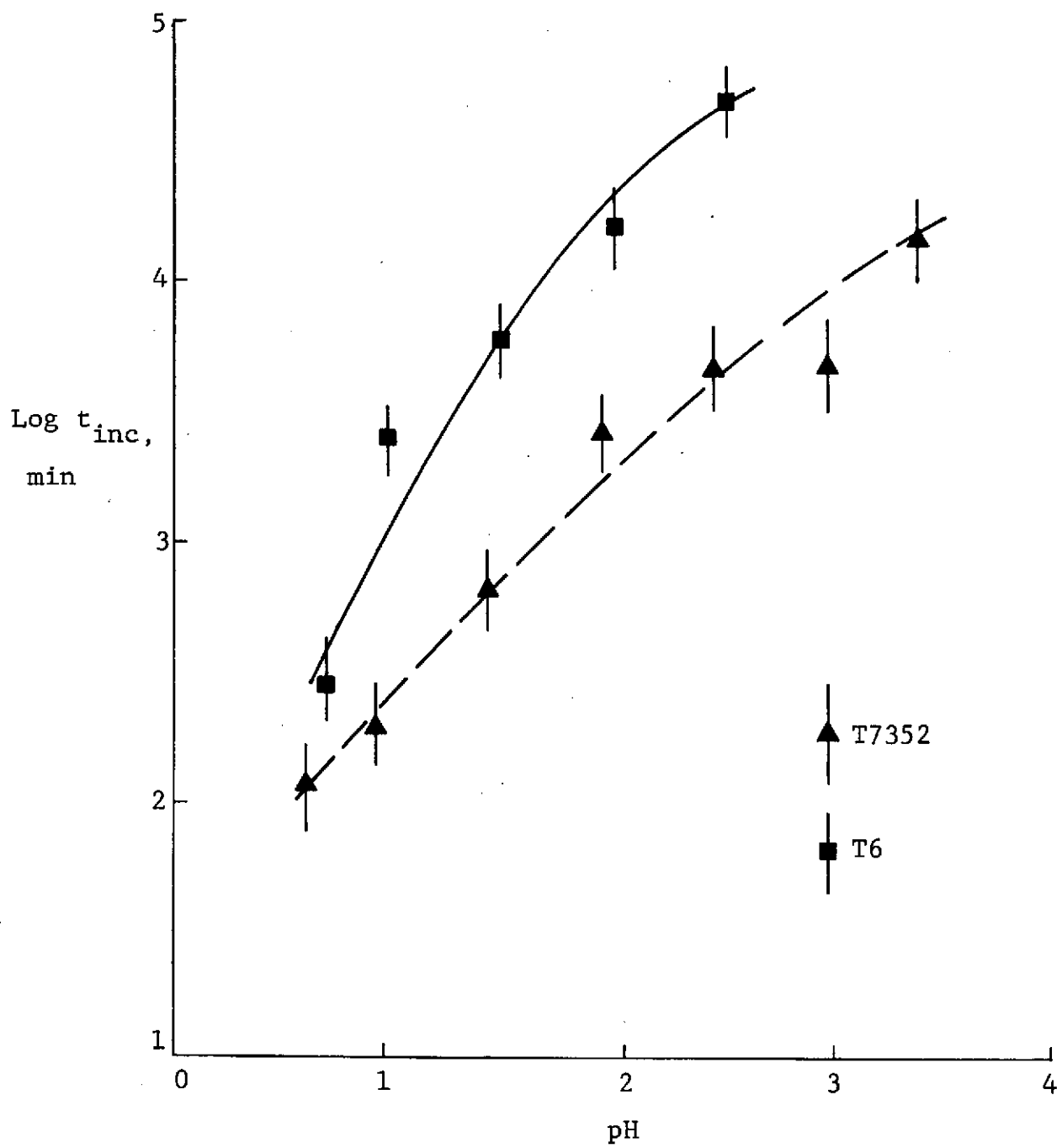
Fig. 21   Effect of pH on the Crack Initiation Time of
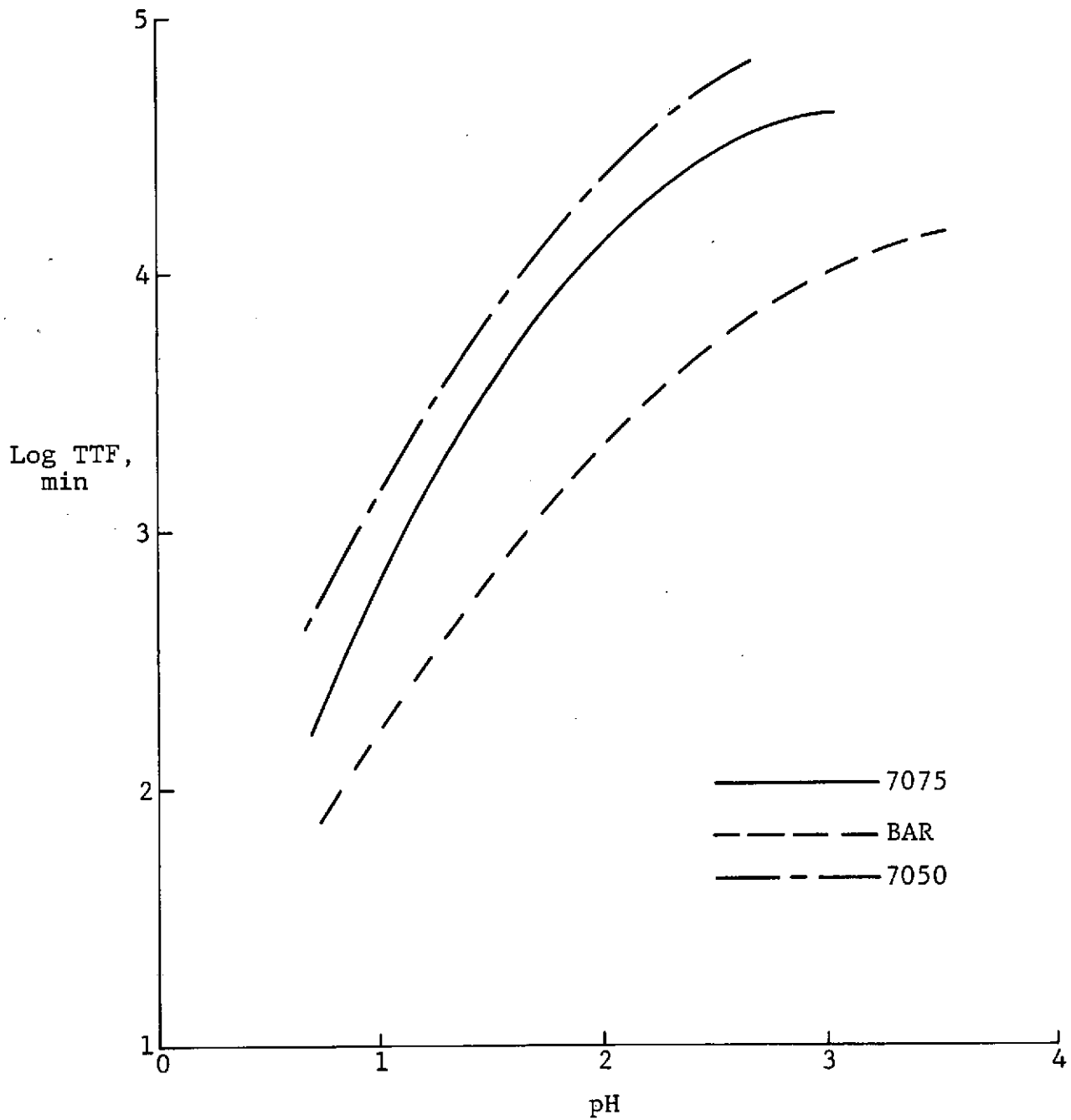Highest Strength and Overaged 7050 Aluminum
Alloy
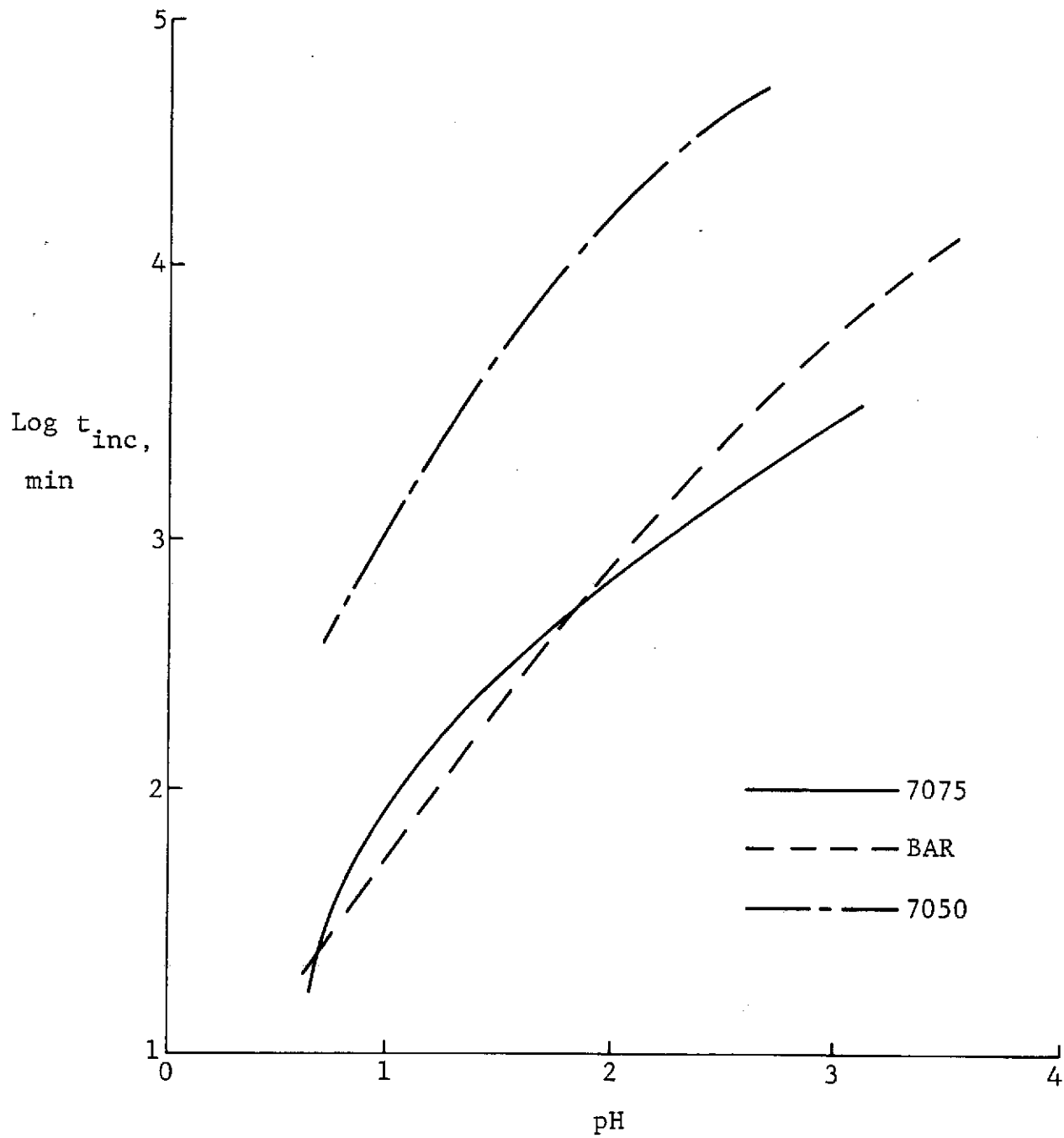
Fig. 22   Comparison of the Crack Initiation Time for the
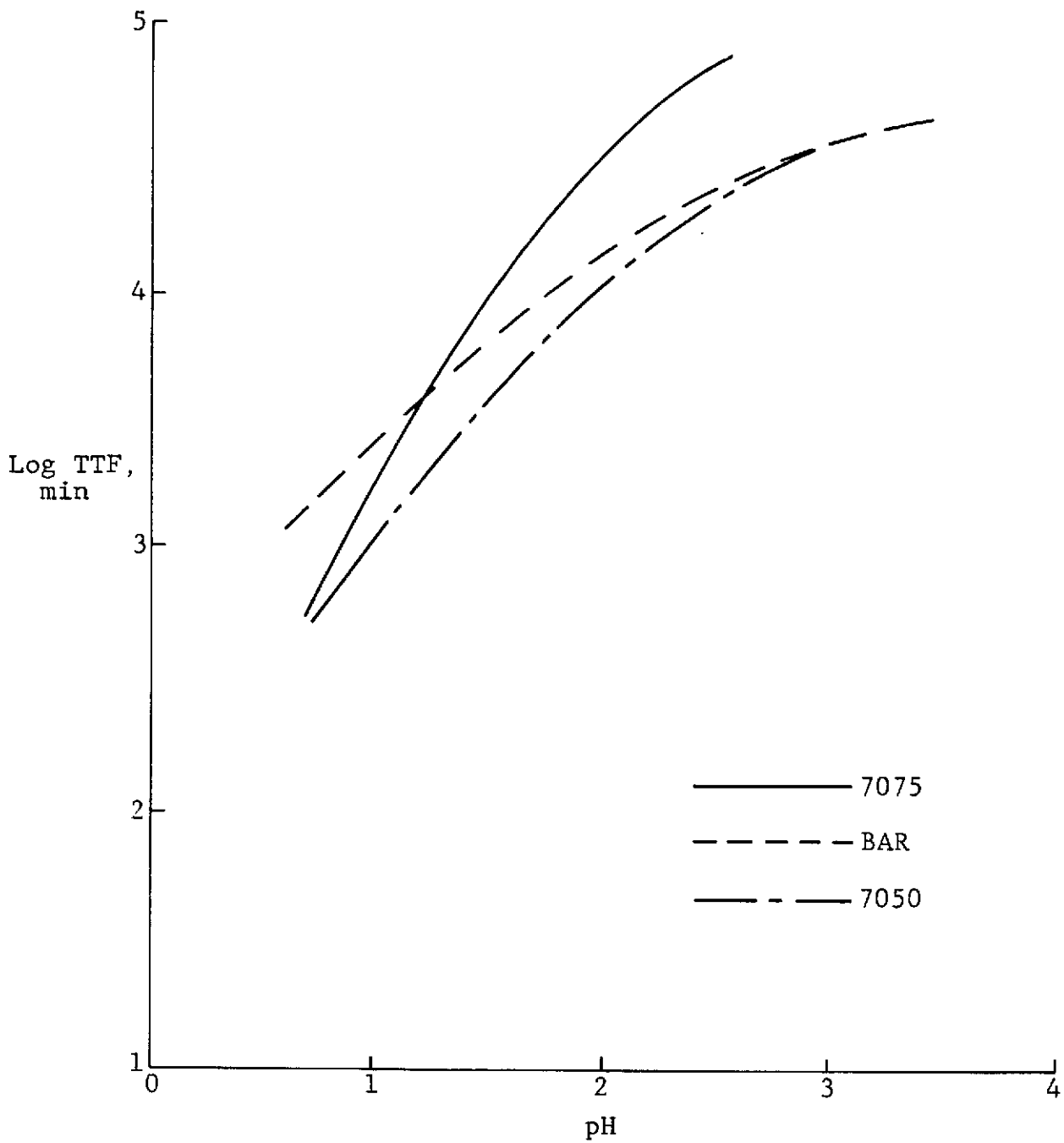Highest Strength Tempers of 7075, BAR, and 7050
Aluminum Alloys
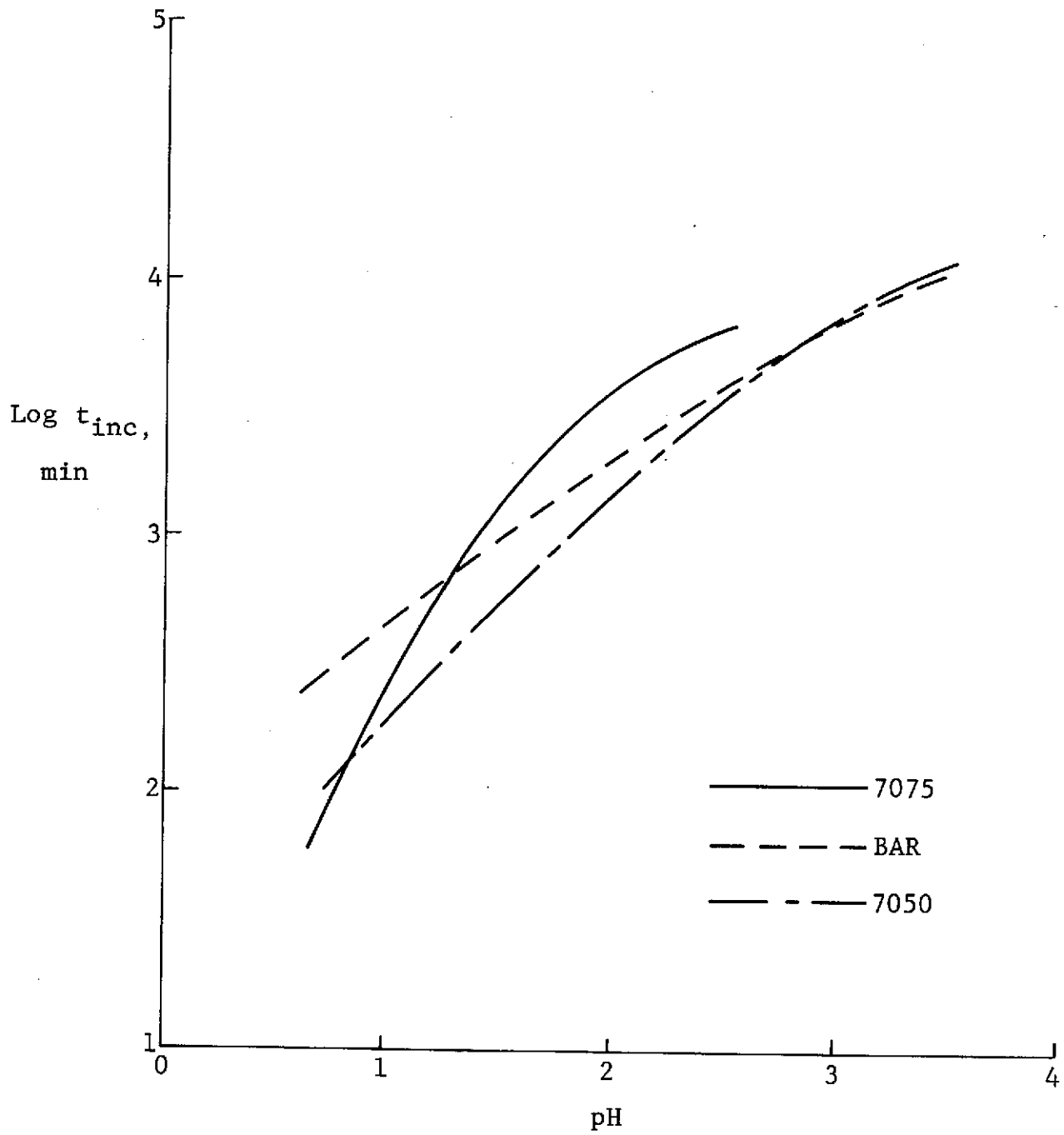
Fig. 23   Comparison of the Crack Initiation Time for the
Overaged Tempers of 7075, BAR, and 7050 Aluminum
Alloys

44

x = Synthetic Sea Water (pH = 8.2)
0 = 3.5 Percent NaCl Solution (pH = 6.8 - 7.2)
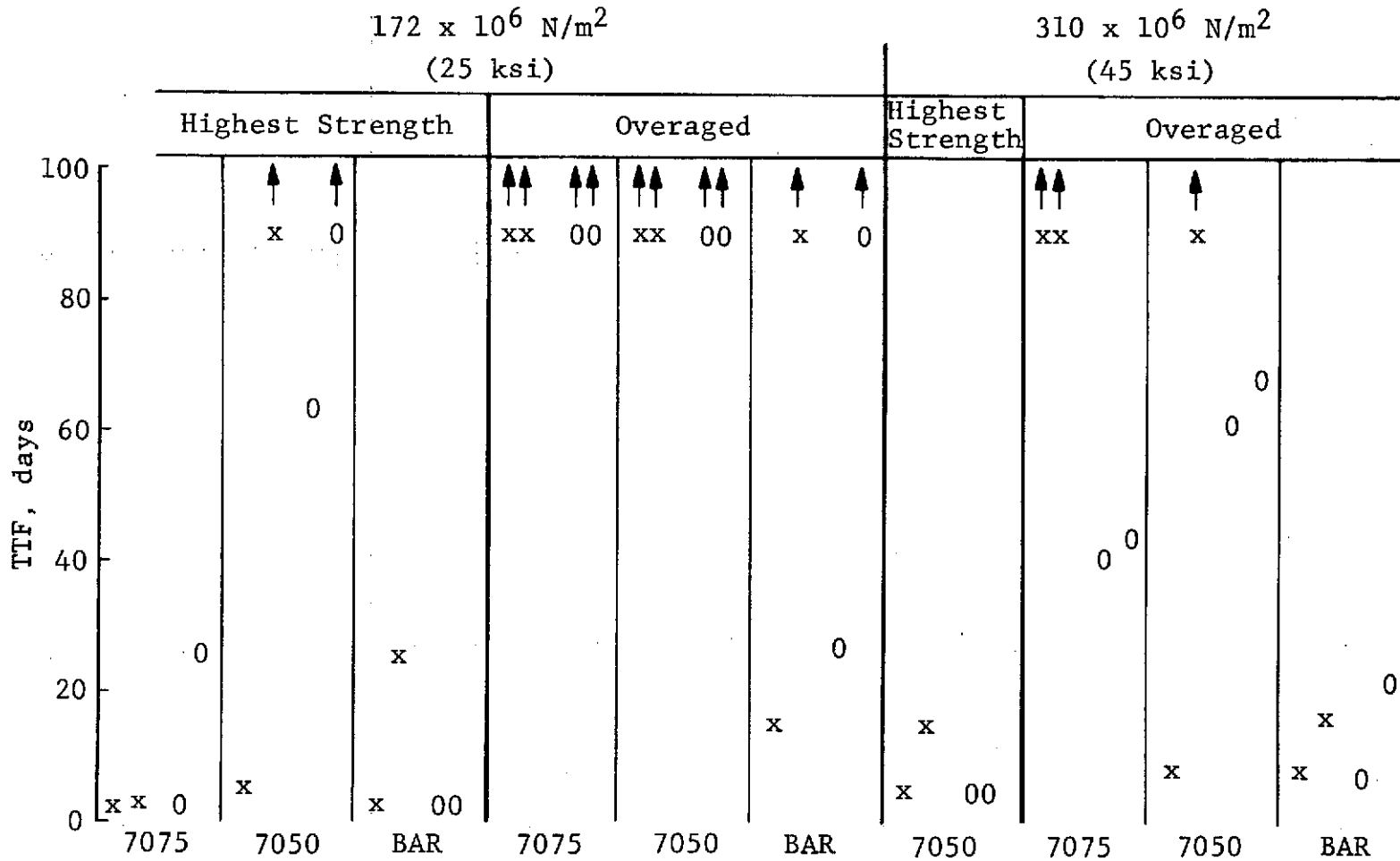


Fig. 24   Alternate Immersion Stress Corrosion Test Results
for Highest Strength and Overaged Tempers of 7075,
7050, and BAR Aluminum Alloys

# 5. DISCUSSION

## A. Mechanical Properties

One of the interesting observations in this study concerns the relatively high strength of the 7050-T6 alloy. This temper was obtained by duplex aging and has the highest strength of the six tempers evaluated. The unusual aspect of 7050-T6 lies in the matrix microstructure associated with highest strength. Previous investigation has shown that highest strength in 7000 series commercial aluminum alloys is related to a predominant G.P. zone matrix with slight amounts of $\eta'$ phase (Refs. 5-7). Strengthening in these alloys has thereby been attributed to the number and distribution of coherent G.P. zones. However, the matrix microstructure of 7050-T6 consists of approximately equal amounts of G.P. zones and $\eta'$ phase, as indicated in Table 3 and Fig. 4 and would appear to be representative of a slightly overaged condition. We singly aged 7050 at $120°C$ for 24 hours after solution treatment and water quenching to obtain a predominately G.P. zone matrix. This treatment led to mechanical properties comparable to that of 7075-T651. The unusual matrix microstructure for highest strength in 7050-T6 is substantiated by DSC results, shown in Table 4. The 7050-T6 has a higher dissolution peak temperature and lower dissolution energy than any of the other highest strength tempers examined. Peak dissolution temperature is an approximate indicator of the stability of existing precipitates. Highest peak temperatures occur for $\eta'$ dissolution. The relatively high dissolution peak temperature for 7050-T6 is, therefore, an indication of the presence of greater amounts of $\eta'$ than exists in the other highest strength tempers. Earlier work on 7075 (Ref. 6) showed that hardness, which is related to mechanical strength, increases with increasing matrix precipitate dissolution energy. This relationship was considered to be based on the presence of a predominant G.P. zone matrix. However, the energy associated with G.P. zone and $\eta'$ dissolution in 7050-T6 is lower than that of any of the other highest strength tempers and comparable to the dissolution energy of the overaged tempers.

Some understanding of the anomalous mechanical behavior of 7050-T6 may be obtained by considering the activation

entropy results in Table 4. A low activation entropy is indicated for 7050-T6 based on its matrix precipitate constituency. If we assume that the entropy of the activated complex state for all the tempers described in Table 4 is approximately equivalent, the low $\Delta S^{\ddagger}$ value for 7050-T6 suggests that the precipitate size distribution in this material is relatively uniform. This could be a principal factor contributing to the anomalously high strength of 7050-T6.

Another interesting factor that may contribute to mechanical properties concerns the grain size of these materials. A significant difference in grain size is evident between 7075 and recently developed BAR and 7050. For 7075, grain sizes are of the order of 95 to 157$\mu$m, whereas the other alloys have grain sizes in the 5-8$\mu$m range. This large difference would be of importance to those properties that are grain size dependent. For example, if we consider the tensile strength of a 7075 alloy with a 5$\mu$m grain size, a 696 x $10^6$N/m$^2$ (101 ksi), tensile strength could be predicted if extrapolation of the Hall-Petch relationship (tensile strength $\alpha d^{-\frac{1}{2}}$) is valid. Such extrapolation is based on previous work for the effect of average grain size on the mechanical properties of 7075 (Ref. 9).

## B. Stress Corrosion Behavior

### 1. Crack Propagation

Correlation of the overall susceptibility parameter, TTF, to a single microstructural factor was not possible for the tempers studied. However, it is possible to consider the role of microstructure on the initiation and propagation of stress corrosion attack. Our earlier work on 7075 aluminum alloy has shown that grain boundary precipitate interparticle spacing, d, is of primary importance to the propagation of stress corrosion cracking (Ref. 5); at pH = 3.0, the crack propagation time increases with increasing interparticle spacing. However, consideration of the present results for 7075, BAR, and 7050 aluminum alloys indicates that the crack propagation time cannot be directly related to interparticle spacing (see Table 3 and Figs. 17 and 18). For example, 7075-T651, which has the smallest grain boundary precipitate interparticle spacing, has the longest crack propagation time

for the highest strength tempers. In addition, BAR-T7 has the largest grain boundary precipitate interparticle spacing and the shortest crack propagation time for the overaged tempers. It is therefore apparent that crack propagation time is not totally dependent upon grain boundary interparticle spacing.

For both highest strength and overaged tempers, $t_p$ for 7075 is greater than that of 7050 and BAR, as shown in Figs. 17 and 18. The average grain size of 7075 is also approximately 20 times larger than that of 7050 and BAR. Since the percentage of grain boundary area per unit volume increases as the grain size decreases, grain size may be a factor of importance to the crack propagation time. This would imply that for comparable interparticle spacing, a coarse grained material would be less susceptible to crack propagation than a finer grained material. Results for 7075, 7050, and BAR are consistent with this interpretation. Grain refinement has also been reported to enhance the corrosion fatigue of 7075 in a 3.5 percent NaCl solution environment (Refs. 61 and 62).

The contribution of grain size to crack propagation does not refute the role of grain boundary precipitate interparticle spacing to crack propagation. Comparison of the crack propagation time for the highest strength and overaged tempers of 7075, BAR, and 7050 (Figs. 14-16, respectively) indicates that for a particular alloy the crack propagation time is shorter in the highest strength than in the overaged temper. Since the grain size of the highest strength and overaged temper of each alloy is the same, and the highest strength temper of each alloy has the smaller grain boundary precipitate spacing, this confirms the importance of interparticle spacing within materials of constant grain size.

It is possible to assess the effect of interparticle spacing on the propagation time by normalizing $t_p$ for grain size. This can be accomplished by calculating the change in $t_p$ that corresponds to an observed change in interparticle spacing for an alloy of constant grain size. Such changes can be obtained by a comparison of $t_p$ for the highest strength and overaged tempers of the three

48

alloys described in Figs. 14-16. This is shown in Fig. 25 for a plot of $\Delta t_p$, that is, $t_p$ (overaged temper) $-t_p$ (highest strength temper), versus $\Delta d$; that is, d (overaged temper) $-d$ (highest strength temper) for 7075, BAR and 7050 at a pH of 2.5. Previously obtained data (Ref. 5) for 7075 specimens that contained different interparticle spacings are also compared with 7075-T7351. Comparison is made at 2.5 pH for the following reasons: 1) it is the highest pH level at which testing was carried out on 7050-T6 and 7075-T7351; 2) it is approximately equal to the pH observed at the crack tip of 7075 aluminum alloy during stress corrosion attack (Ref. 63); and 3) it is beyond the highly pH dependent region where a dissolution mechanism of attack is suspected (Ref. 36). The agreement of the data to a least square linear fit indicates that the change in $t_p$ is dependent upon $\Delta d$ in all cases. The extrapolated zero intercept is also consistent with the argument regarding the effect of interparticle spacing on $t_p$. Therefore, the propagation of stress corrosion cracking at constant grain size can be related to grain boundary interparticle spacing.

## 2. Crack Initiation

There appears to be only slight differences in the $t_{inc}$ as a function of pH among five of the six tempers examined. For 7050-T6, however, relatively long times are necessary for crack initiation over the entire pH range investigated. These long times are of particular interest since they are primarily responsible for this material's high overall stress corrosion resistance, and they represent a desired characteristic that may be applied to other aluminum alloys. Although the PFZ width is smallest for 7050-T6, this small difference cannot account for the very large difference in crack initiation time between this temper and the others studied. In fact, no direct correlation can be made between $t_{inc}$ and the matrix and grain boundary properties listed in Table 3. It is likely that another factor, possibly electrochemical potential, is significant to crack initiation.

The sample emf when measured relative to a saturated calomel reference electrode is an indication of the tendency
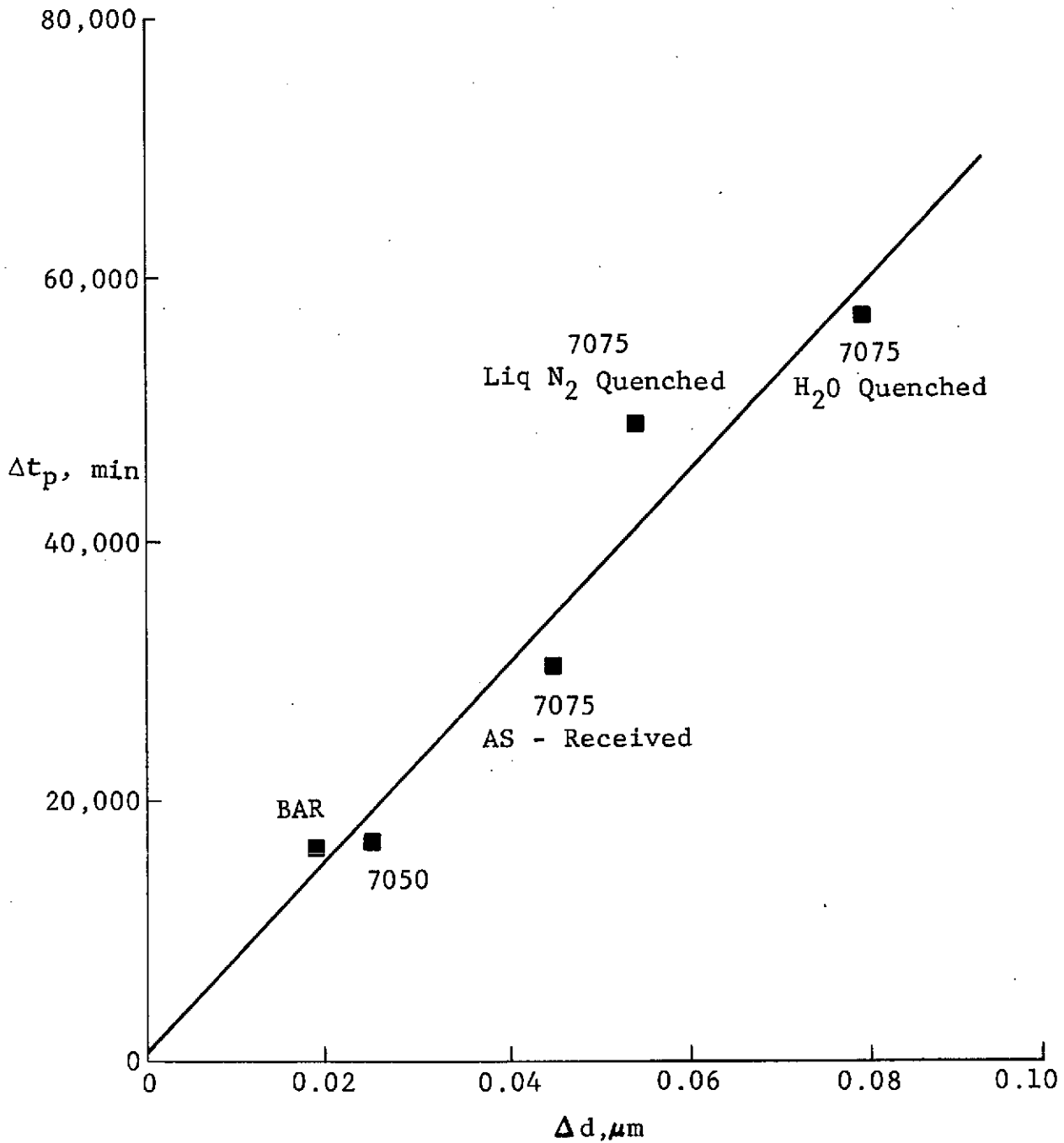
Fig. 25 Relationship Between the Change in Grain Boundary Interparticle Spacing at Constant Grain Size and the Corresponding Change in Crack Propagation Time

of the elements in solid solution to undergo oxidation. This oxidation potential is dependent upon the concentration of $Al(H_2O)_6^{+3}$ and $H_3O^+$ in solution, both of which are buffered in the initial chloride test solution and are constant for each temper investigated. Therefore, the oxidation of the aluminum solid solution and the corresponding reduction of hydrogen ion will not change the total concentration of these species during the crack incubation period. Thus the emf at a particular pH level is primarily dependent on the ease of dissolution of the elements in solid solution. Differences in emf between tempers could be partially responsible for the significant difference in $t_{inc}$ noted above. Additional work is being performed to elucidate the effect of emf on $t_{inc}$.

3. Overall Susceptibility

Although 7075-T73 appears to have highest resistance to stress corrosion attack in both alternate immersion and our laboratory testing, differences are apparent between test results for other tempers. The 7050-T6 material appears comparable to 7075-T7351 in our laboratory testing, yet it is not comparable in alternate immersion tests at both $172 \times 10^6$ and $310 \times 10^6 N/m^2$ (25 and 45 ksi). In addition, 7050-T6 appears to have greater resistance to stress corrosion attack than 7050-T73 in our laboratory tests, whereas the opposite is true in alternate immersion testing. Similarly, 7075-T651 and 7050-T7352 appear comparable in the pH range of our laboratory testing, whereas alternate immersion test results indicate far greater stress corrosion resistance for 7050-T7352. These, as well as other differences, point out the importance of testing conditions on the relative susceptibility of these tempers. In both our laboratory tests and alternate immersion testing, specimens were stressed in the short transverse direction, but the specimen configuration as well as the conditions of exposure were different. However, it is felt that a major difference between the testing conditions lies in the environment acidity. Our laboratory testing was performed over a 0.7-3.4 pH range, whereas the alternate immersion tests were run at either 6.8-7.2 pH or at 8.2 pH. The curves of TTF versus pH shown in Figs. 12 and 13 indicate that differences in pH dependence above a

pH of 3.4 among the tempers studied may lead to reversals in the relative susceptibilities at higher pH. For example, the TTF for 7050-T7352 may continue to increase with increasing pH whereas that of 7050-T6 may become independent of pH. This would lead to a crossover in the TTF versus pH curves and would be consistent with the alternate immersion results. In many cases, the existing environment pH may not be obvious. Brown et al. (Ref. 63) have found a pH of about 3.0-3.5 at the tip of a stress corrosion crack in 7075 aluminum alloy exposed to a 3.5 percent NaCl solution of pH 6.5. It is important, therefore, that the effect of environment pH be considered in any comparison of relative susceptibilities.

# 6. CONCLUSIONS

Stress corrosion crack propagation in 7050, BAR, and 7075 aluminum alloys was found to be dependent on grain boundary precipitate spacing; larger spacing enhances resistance to crack propagation. Another factor, probably grain size, must also be considered in a generalized relationship between microstructure and susceptibility to crack propagation.

The 7050-T6 material was found to exhibit far greater resistance to stress corrosion crack initiation than any of the other tempers studied. Resistance to crack initiation does not appear related to any microstructural features and may be a function of electrochemical potential produced by the dissolution of solid solution in the vicinity of the grain boundary.

Overall resistance to stress corrosion attack over a 0.7-3.4 pH range in an aqueous chloride solution was found to be greatest for 7075-T7351 and 7050-T6. Comparably lower resistance was found for 7075-T651, 7050-T7352, and BAR-T7. The BAR-T6 temper was found to be least resistant to stress corrosion attack. These results are not totally consistent with alternate immersion test results obtained in 6.8-7.2 pH and 8.2 pH environments that indicate 7075-T7351 and 7050-T7352 to be most resistant to attack.

Differences between our laboratory results and alternate immersion results are likely related to the pH of the test environment. Since the pH in the vicinity of cracks differs from that in a solution environment and since the pH of service environments are not well defined, it is important to determine a material's overall resistance to stress corrosion attack as a function of pH.

The 7050-T6 temper was found to have an unusually high mechanical strength in relation to its matrix microstructure. Results of DSC analysis suggest that uniformity of the matrix precipitate size distribution may be responsible for the observed strengthening.

The grain size of BAR and 7050 alloys, both containing a Zr substitution for Cr, is approximately five percent of that in 7075. This reduced grain size may enhance the mechanical strength of these alloys, but it also appears to decrease their resistance to stress corrosion attack.

## 7. RECOMMENDATIONS FOR FUTURE WORK

1. Extend stress corrosion testing to pH = 7 to gain a more complete understanding of the role of pH to the initiation and propagation of cracking and to correlate our test results with those of alternate immersion testing.

2. Characterize the role of electrochemical potential to the initiation of cracking. Included in this area would be the effect of alloying elements, pH and load.

3. Investigate the effect of grain size on stress corrosion crack propagation. This would be accomplished by selecting significantly different grain sizes of 7075 or 7050 material and testing over the pH range of 2.0-7.0.

4. Further investigate the anomalous strengthening mechanism of 7050. This will be accomplished by further DSC characterizations of the 7050 alloy containing matrix microstructures varying from G.P. zones to $\eta' + \eta$.

# 8. REFERENCES

1. Mondolfo, L. F., _Metals Mater._, Vol. 5, p. 95, 1971.

2. Ostermann, F. G. and Reimann, W. H., _ASTM STP 467_, p. 169, 1970.

3. Sprowls, D. O. and Brown, R. H., _Metals Progr._, Vol. 81, No. 4, p. 79, 1962.

4. Sprowls, D. O. and Brown, R. H., _Metals Progr._, Vol. 81, No. 5, p. 77, 1962.

5. Adler, P. N., DeIasi, R., and Geschwind, G., _Met. Trans._, Vol. 3, p. 3191, 1972.

6. Adler, P., Geschwind, G., and DeIasi, R., "Proc. of Third International Conference on Thermal Analysis," Vol. 2, p. 747, Berkhaüser Verlag, Basel, Switzerland, 1972.

7. Sprowls, D. O. and Brown, R. H., "International Conference on Fundamental Aspects of Stress Corrosion Cracking," NACE, p. 466, Houston, Texas, 1969.

8. Hunsicker, H. Y., _Aluminum_, Vol. 1, p. 125, ASM, Metals Park, Ohio, 1967.

9. Geschwind, G., Soltz, G. C., and Adler, P. N., _Corrosion_, Vol. 26, p. 165, 1970.

10. Thomas, G. and Nutting, J., _J. Inst. Metals_, Vol. 88, p. 81, 1959-60.

11. Kelly, A. and Nicholson, R. B., _Progr. Mater. Sci._, Vol. 10, No. 3, p. 216, 1963.

12. Mondolfo, L. F., Gjostein, N. A., and Levinson, D. W., _AIME Trans._, Vol. 206, p. 1378, 1956.

13. Gjonnes, J. and Simensen, C. J., _Acta Met._, Vol. 18, p. 881, 1970.

14. Smith, W. F. and Grant, N. J., _Met. Trans._, Vol. 1, p. 979, 1970.

15. Varly, P. C., Day, M. K. B., and Sendorek, A., _J. Inst. Metals_, Vol. 86, p. 337, 1957-58.

16. Polmear, I. J., _J. Inst. Metals_, Vol. 87, p. 24, 1958-59.

17. Singh, S. N. and Flemings, M. C., _Trans. TMS-AIME_, Vol. 245, p. 1803, 1969.

18. Mulherin, J. H. and Rosenthal, H., _Met. Trans._, Vol. 2, p. 427, 1971.

19. DiRusso, E., Conserva, M., Gatto, F., and Markus, H., _Met. Trans._, Vol. 4, p. 1133, 1973.

20. Ryum, N., _Acta Met._, Vol. 16, p. 327, 1968.

21. Cornish, A. J. and Day, M. K. B., _J. Inst. Metals_, Vol. 99, p. 377, 1971.

22. Kirman, I., _Met. Trans._, Vol. 2, p. 1761, 1971.

23. van Leeuwen, H. P., Schra, L., and van der Vet, W. J., _J. Inst. Metals_, Vol. 100, p. 86, 1972.

24. Thomas, G., _J. Inst. Metals_, Vol. 87, p. 24, 1958-59.

25. Pugh, E. N. and Jones, W. R. D., _Metallurgia_, Vol. 63, p. 3, 1961.

26. McEvily, A. J., Clark, J. B., and Bond, A. P., _Trans. ASM_, Vol. 60, p. 661, 1967.

27. Sedriks, A. J., Slattery, P. W., and Pugh, E. N., _Trans. ASM_, Vol. 62, p. 238, 1969.

28. Sedriks, A. J., Slattery, P. N., and Pugh, E. N., _Trans. ASM_, Vol. 62, p. 815, 1969.

29. Taylor, I. T. and Edgar, R. L., _Met. Trans._, Vol. 2, p. 833, 1971.

30. Holl, H. A., _Corrosion_, Vol. 23, p. 173, 1967.

31. DeArdo, A. J. and Townsend, R. D., _Met Trans._, Vol. 1, p. 2573, 1970.

32. Starke, E. A., Jr., _J. Metals_, Vol. 22, No. 1, p. 54, 1970.

33. Gruhl, N., _Aluminum_, Vol. 38, p. 775, 1962.

34. Gruhl, W. and Cordier, H., _Aluminum_, Vol. 44, p. 403, 1968.

35. Speidel, M., _Phys. Status Solidi_, Vol. 22, K71, 1967.

36. Geschwind, G. and Adler, P. N., International Corrosion Conference 73, Paper No. 97, NACE, Houston, Texas, 1973.

37. Kent, K. G., _J. Aust. Inst. Metals_, Vol. 15, p. 171, 1970.

38. Kent, K. G., _J. Inst. Metals_, Vol. 97, p. 127, 1969.

39. Unwin, P. N. T. and Nicholson, R. B., _Acta Met._, Vol. 17, p. 1379, 1969.

40. Thompson, D. S., AFML-TR-73-18, April 1973.

41. Thompson, D. S. and Levy, S. A., AFML-TR-70-171, August 1970.

42. Hyatt, M. V. and Schimmelbusch, H. W., AFML-TR-70-109, May 1970.

43. Staley, J. T., NASC Contract No. N00019-69-C-0292, January 1970.

44. Staley, J. T., NASC Contract No. N00019-70-C-0118, November 1970.

45. Staley, J. T., NASC Contract No. N00019-71-C-0131, May 1972.

46. Staley, J. T., AFML-TR-70-256, November 1970.

47. Staley, J. T., AFML Contract F33615-69-C-1644, January 1970.

48. Bryant, A. J., J. Inst. Metals, Vol. 94, p. 94, 1966.

49. Baba, Y., Trans. Jap. Inst. Metals, Vol. 9, p. 507, 1968.

50. DiRusso, E., Report No. 16269 ISML (Experimental Inst. of Light Metals), Navara, July 1966.

51. Conserva, M., DiRusso, E., and Caloni, I., Met. Trans., Vol. 2, p. 1227, 1971.

52. Thompson, D. S., Subramanya, B. S., and Levy, S. A., Met. Trans., Vol. 2, p. 1149, 1971.

53. Hunsicker, H. Y., Staley, J. T., and Brown, R. H., Met. Trans., Vol. 3, p. 201, 1972.

54. Conserva, M. and Fiorini, P., Met Trans., Vol. 4, p. 857, 1973.

55. Smith, W. F. and Grant, N. J., Met Trans., Vol. 2, p. 1333, 1971.

56. Staley, J. T., Hunsicker, H. Y., and Schmidt, R., ASM-AIME Fall Meeting, 1971, Detroit, Alcoa Publication.

57. Baxter, R. A. in Thermal Analysis, Vol. I, ed. by R. F. Schwenker, Jr. and P. D. Garn, Academic Press, N.Y. (1969) p. 65.

58. Swalin, R., Thermodynamics of Solids, J. Wiley, New York (1963), p. 60.

59. Frast, A. A. and Pearson, R. G., Kinetics and Mechanism, J. Wiley and Sons, Inc., N. Y. (1953), p. 98.

60. Rostoker, W. and Dvorak, J. R., "Interpretation of Metallographic Structures," Academic Press, New York, p. 203, 1965.

61. Selines, R. J. and Pelloux, R. M., <u>Met. Trans</u>., Vol. 3, p. 2525, 1972.

62. Stoltz, R. E. and Pelloux, R. M., <u>Met. Trans</u>., Vol. 3, p. 2433, 1972.

63. Brown, B. F., Fujii, C. T., and Dahlberg, E. P., <u>J. Elect. Soc</u>., Vol. 116, p. 218, 1969.